

1
2
3
4
5
6
7
8
9
10
11
12
13
14
15
16
17
18
19
20
21
22
23
24
25
26
27
28
29
30
31
32
33
34
35
36

Identifying analogues for Melimoyu, a long-dormant and data-limited volcano in Chile, through hierarchical clustering

Burgos, V*^{1,2}, Jenkins, S.F.^{1,2}, Bono Troncoso, L.³, Perales Moya, C. V.³, Bebbington, M.⁴, Newhall, C.⁵, Amigo, A.³, Prada Alonso, J.⁶, Taisne., B.^{1,2}

¹Earth Observatory of Singapore, Singapore

²Asian School of the Environment, Nanyang Technological University, Singapore

³Red Nacional de Vigilancia Volcánica. Servicio Nacional de Geología y Minería (SERNAGEOMIN). Santiago, Chile.

⁴School of Agriculture and Environment, Massey University, Palmerston North, New Zealand

⁵Mirisbiris Garden and Nature Center, Philippines

⁶Escuela Politécnica Superior, Universidad Autónoma de Madrid, Madrid, Spain

Burgos, V*

burg0001@e.ntu.edu.sg

April 21, 2023

This manuscript is a non-peer reviewed preprint submitted to Frontiers in Earth Science and has not yet been accepted for publication. Subsequent versions of this manuscript may have different content. If accepted, the final version of this manuscript will be available via the ‘Peer-reviewed Publication DOI’ link on its EarthArXiv web page. Please feel free to contact us with any comments or feedback about our study.

V2: Updated supplementary material links

Abstract

Melimoyu is a long-dormant and data-limited volcano in the Southern Volcanic Zone (SVZ) in Chile with only two confirmed Holocene eruptions (VEI 5). Determining the frequency-magnitude relationship for Melimoyu is challenging due to data scarcity. To supplement the eruption records, we identify analogue volcanoes for Melimoyu (i.e., volcanoes that behave similarly and are identified through shared characteristics) using a quantitative and objective approach. Firstly, we compiled a global database containing 181 variables describing the eruptive history, tectonic setting, rock composition, and morphology of 1428 volcanoes. This database was filtered primarily based on data availability into an input dataset comprising 37 numerical variables for 438 subduction zone volcanoes.

37 Then, we applied Agglomerative Nesting, a bottom-up hierarchical clustering algorithm on three
38 datasets derived from the input dataset: i) raw data, ii) output from a Principal Component Analysis,
39 and iii) weighted data tuned to minimise the dispersion in the absolute probability per VEI. Lastly, we
40 identified the best set of analogues by analysing the dispersion in the absolute probability and applying
41 a set of criteria deemed important by the local geological service, SERNAGEOMIN, and VB. Our
42 analysis shows that the raw data generates a low dispersion and the highest number of analogues (n=20).
43 More than half of these analogues are in the SVZ, suggesting that the tectonic setting plays a key role
44 in the clustering analysis. The f -M relationship modelled from the analogue's eruption data shows that
45 if Melimoyu has an eruption, there is a 49% probability (50th percentile) of it being $VEI \geq 4$. Meanwhile,
46 the annual absolute probability of a $VEI \leq 1, 2, 3, 4$, and $VEI \geq 5$ eruption at Melimoyu is 4.82×10^{-4} ,
47 1.2×10^{-3} , 1.45×10^{-4} , 9.77×10^{-4} , and 8.3×10^{-4} (50th percentile), respectively. Our work shows the
48 importance of using numerical variables to capture the variability across volcanoes and combining
49 quantitative approaches with expert knowledge to assess the suitability of potential analogues.
50 Additionally, this approach allows identifying groups of analogues and can be easily applied to other
51 cases using numerical variables from the global database. Future work will use the analogues to
52 populate an event tree and define eruption source parameters for modelling volcanic hazards at
53 Melimoyu.

54

55 **Keywords:** Analogues, Data-limited, Eruption probability, Frequency-Magnitude relationship, Long-
56 dormant, Hierarchical clustering, Machine learning, Principal Component Analysis.

57

58 **Abbreviations:** AGglomerative NESTing (AGNES), Cumulative Distribution Function (CDF), Global
59 Volcanism Program (GVP), frequency-Magnitude (f -M), Interquartile Range (IQR), Liquiñe-Ofqui
60 Fault Zone (LOFZ), Magnitude (M), Principal Component (PC), Principal Component Analysis (PCA),
61 Pyroclastic Density Current (PDC), Relative Completeness Date (RCD), Southern Volcanic Zone
62 (SVZ), Volcanic Explosivity Index (VEI), Volcanoes of the World (VOTW)

63 1. Introduction

64 Volcanoes with limited data on past eruptions are prevalent in global catalogues, such as the Volcanoes
65 of the World VOTW (GVP, 2013) or LaMEVE database (Crosweller et al., 2012). Melimoyu (Chile),
66 with just two confirmed Holocene eruptions, both VEI 5 (Geoffroy et al., 2018), is one of these data-
67 limited volcanoes. We consider Melimoyu a long-dormant volcano (i.e., as defined in Burgos et al.
68 (2022a): “an active or potentially active volcano without recorded eruptions within the last 100 years”);
69 the last confirmed eruption took place more than 1800 years ago. According to the Specific Volcanic
70 Risk Ranking of Active Volcanoes of Chile (SERNAGEOMIN, 2019), Melimoyu is a Volcanic System
71 Type II (i.e., high-risk volcanic system or volcanic system with recent anomalous activity), ranking 28th

72 out of 92 Chilean active volcanoes. The most recent, and only detected unrest at Melimoyu, took place
73 in May 2010, when there was an increase in the seismic activity, leading to the Alert Level being raised
74 to Green Level 2 (GVP, 2010) out of the seven alert levels available at that time (i.e., Green 1 and 2;
75 Yellow 1 and 2; and Red 1, 2, and 3 (Bono, L. and Perales, C. personal communication)).

76 Estimating how often a data-limited volcano like Melimoyu erupts and assessing its volcanic hazards
77 is challenging since the range of past eruptive styles is not well known (Loughlin et al., 2015). Several
78 factors can prevent us from having comprehensive eruption records, such as historical events and socio-
79 cultural factors, the capacity to conduct geological studies, the presence of submarine volcanism,
80 environmental conditions, and accessibility to the study areas (Burgos et al., 2022b; Mead and Magill,
81 2014; Siebert et al., 2011). Ideally, we can improve the eruption record by collecting new field data
82 while the volcano is dormant and there is no imminent threat of reactivation. In Melimoyu, a detailed
83 fieldwork campaign was carried out by Geoffroy (2017), which focused on characterising the deposits
84 from the two known Holocene eruptions.

85 Despite these recent efforts, the data available for Melimoyu are still scarce. The main causes are the
86 high erosion rate in the Patagonian Andes caused by the climatic conditions, especially during glacial
87 periods, resulting in poorly preserved deposits, and the permanent ice cap covering most of Melimoyu's
88 edifice (Geoffroy et al., 2018; Herman and Brandon, 2015). In addition, the region of Aysén was
89 occupied only from the late 19th century (Marín, 2014), which could have contributed to the lack of
90 historical accounts of any potential activity in Melimoyu. Therefore, we must rely on analogue
91 volcanoes (i.e., volcanoes we expect to behave similarly and which are identified through shared
92 characteristics) to supplement the eruption record.

93 Analogue volcanoes have been typically defined based on location, tectonic setting, morphology,
94 magma type, eruption style, or a combination of these factors for i) assessing local and regional volcanic
95 hazards (e.g., Jenkins et al., 2012b; Lindsay and Robertson, 2018; Mastin et al., 2009; Newhall, 1982;
96 Newhall and Pallister, 2015; Sandri et al., 2014, 2012; Tennant et al., 2021; Tierz et al., 2020); ii)
97 estimating frequency-Magnitude (f - M) relationship (e.g., Hayes et al., 2022; Jenkins et al., 2012a, 2022;
98 Rodado et al., 2011; Runge et al., 2014; Sheldrake and Caricchi, 2017; Solow, 2001; Whelley et al.,
99 2015) s; iii) conducting probabilistic eruption forecasts (e.g., Bebbington, 2014; Bebbington and
100 Jenkins, 2022; Marzocchi et al., 2004; Sheldrake, 2014), and iv) identifying unrest patterns (e.g.,
101 Acocella et al., 2015; Newhall et al., 2017).

102 One commonly used approach to identify analogues is classifying volcanoes into categorical classes.
103 For example, Whelley et al. (2015) proposed five categories of volcanoes that combined the
104 morphology of the edifice, the state of the activity, and the dimension of the summit crater. One
105 limitation of using categorical classifications is that numerous volcanoes meet the criteria of a given
106 category. For example, Whelley et al. (2015) identified 102 volcanoes as well-plugged just in SE Asia.

107 Hayes et al. (2022) showed that classifying volcanoes into broad categories result in large uncertainty
108 in the f - M relationship estimations of SE Asia volcanoes, especially when using global analogues.
109 Similarly, Bebbington and Jenkins (2022) demonstrated that intra-eruption forecasting did not improve
110 when using data from analogues identified from categorical classes of morphology or composition
111 instead of the entire dataset once the current activity is accounted for.

112 Several studies have proposed different quantitative approaches to identifying analogue volcanoes in
113 the last two decades. For example, Hone et al. (2007) carried out a cladistic classification of volcanoes
114 in Honshu (Japan) by combining multiple characteristics split into states (e.g., the amount of basalt
115 (compositional type characteristic) is divided into five states that range from none to substantial) and
116 assigning them individually to each volcano. This approach would be time-consuming to apply at a
117 global scale (Hone et al., 2007). Sobradelo et al. (2010) classified analogous calderas into three groups
118 with different geodynamic environments by analysing the caldera area. Tierz et al. (2019) developed
119 VOLCANS, which combines up to five weighted volcanological criteria to obtain an analogy metric.
120 VOLCANS is designed to identify analogues for one target volcano at a time since the analogy metric
121 measures the similarity between a given volcanic system in their database and the target volcano (i.e.,
122 it does not provide groups of analogue volcanoes). A limitation of VOLCANS is that the weights
123 assigned to each criterion are selected subjectively by the user. This step can be crucial since the
124 proposed analogues differ depending on the weighting scheme (Tierz et al., 2019), generating notably
125 different eruption probability estimates (Tierz et al., 2020). More recently, Wang et al. (2022)
126 introduced the concept of statistical analogues and proposed using a Weibull renewal process to identify
127 volcanoes with similar inter-eruption repose times. This new approach was successfully implemented
128 for forecasting eruptions at Tongariro (New Zealand), a well-studied volcano with 79 confirmed
129 Holocene eruptions in the VOTW database (GVP, 2013). However, the applicability for data-limited
130 volcanoes has yet to be tested since it requires several observations (i.e., eruption dates) to estimate the
131 three model parameters with any degree of precision.

132 In this study, we propose using hierarchical clustering to identify analogues quantitatively and
133 objectively. Clustering algorithms have been used in volcanology for various applications, such as
134 detecting patterns in seismic data (e.g., Duque et al. (2020) and Unglert et al. (2016)) or classifying
135 volcanoes based on morphometric data (e.g., Grosse and Kervyn (2018) and Paguican et al. (2021)).
136 One of the main challenges when clustering data is that the most used algorithms, such as K-mean,
137 PAM, or GMM (Xu and Tian, 2015), require the optimal number of clusters to be selected before the
138 application. To avoid this step, we used AGglomerative NESTing (AGNES), a form of bottom-up
139 hierarchical clustering that produces a dendrogram without having to pre-define the number of clusters.
140 This advantage allows us to cut the dendrogram at a height that produces a cluster containing at least
141 50 potential analogues for Melimoyu. Another important advantage of using AGNES is that the

142 dendrogram can be used to identify analogues for multiple target volcanoes at the same time, which
143 could also help us understand why volcanoes are being grouped in each cluster.

144 Our application of hierarchical clustering focuses on identifying analogues for Melimoyu for estimating
145 the frequency-magnitude relationship. Finding analogues for data-limited volcanoes can be challenging
146 since we cannot use the eruptive history of other volcanoes to identify analogues, especially if we want
147 to avoid clustering volcanoes based on the number of available eruptions. For this reason, we rely on
148 numerical variables that describe the tectonic setting, morphology, and rock composition to find similar
149 volcanoes with the assumption that these factors control eruption rates and/or reflect the eruptive style
150 and recent eruptive activity (Acocella, 2014; Acocella and Funicello, 2010; Hughes and Mahood, 2011,
151 2008a; Sheldrake et al., 2020; Weber and Sheldrake, 2022; Whelley et al., 2015). We compiled 181
152 variables for 1428 volcanoes from multiple sources and applied AGNES to a selection of 37 numeric
153 variables describing the rock composition, tectonic setting, and morphology of 438 subduction zone
154 volcanoes (see Section 3.2).

155 The analysis consisted of three steps. First, a sensitivity analysis was performed using three different
156 datasets to assess how the input data influences the definition of analogues and the performance of the
157 clustering. Then, we compared the dispersion in the absolute eruption probability (i.e., the annual
158 probability of an eruption of a given VEI) from the three sets of potential analogues. Next, the
159 suitability of the analogue volcanoes was assessed by applying specific criteria considered important
160 by SERNAGEOMIN and VB for being an analogue of Melimoyu (see Section 4.3), such as having a
161 history of large explosive eruptions ($VEI \geq 4$) in the Holocene. Lastly, the eruption records from the
162 analogues were used to model the f -M relationship given by the absolute and conditional (i.e., relative
163 probability of an eruption of a given VEI, conditional on an eruption has already taken place)
164 probability.

165 This approach allows us to objectively group volcanoes based on similar volcanic characteristics, assess
166 the goodness of the clustering using quantitative metrics while accounting for expert knowledge, and
167 quantify the uncertainty in our analogue-derived estimates of eruption probabilities. Furthermore, we
168 provide the global database (accessible in supplementary material 1) with 181 variables and 1428
169 volcanoes so that our approach can be easily applied to other volcanoes or a different selection of
170 variables.

171 In summary, this paper aims to:

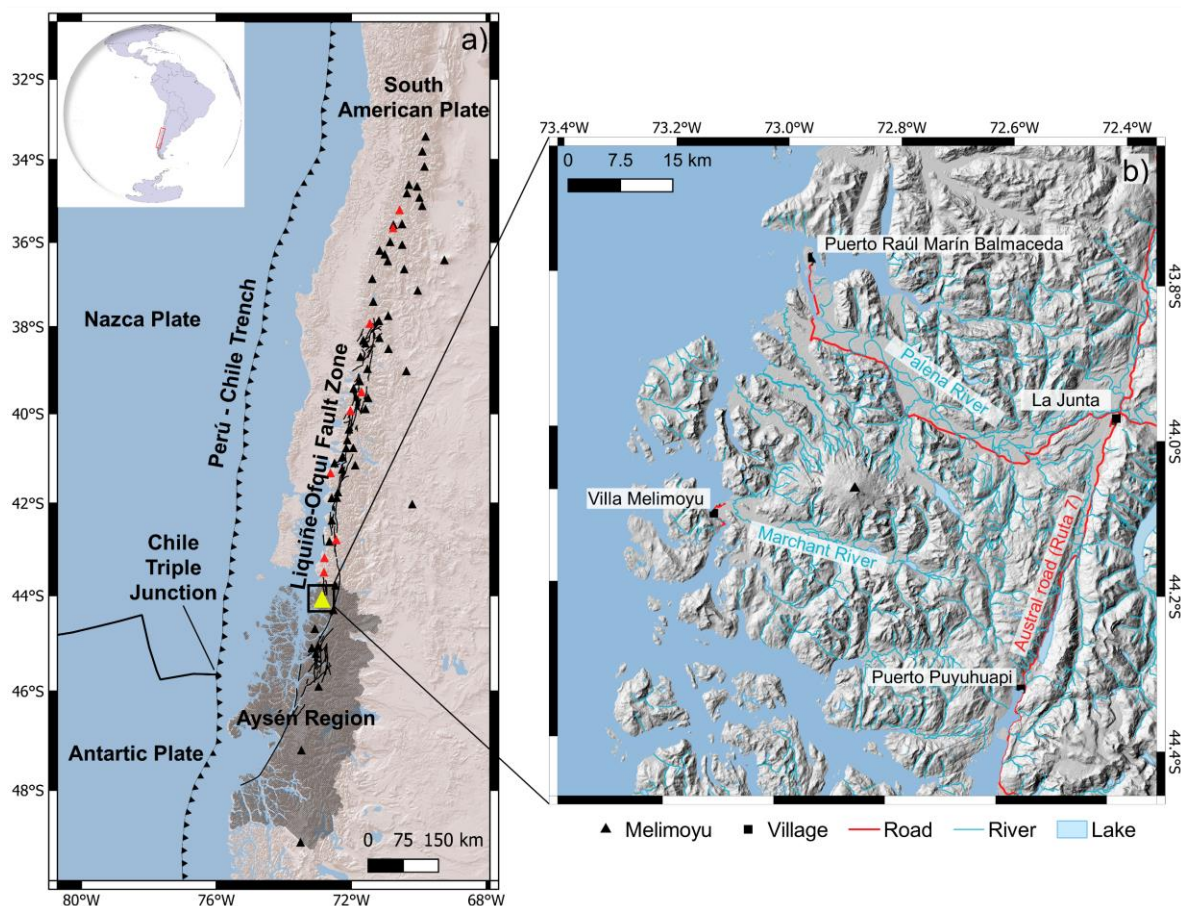
- 172 1. Automatically identify analogue volcanoes quantitatively and objectively for Melimoyu.
- 173 2. Assess the influence of the input data on the clustering results through a sensitivity analysis.
- 174 3. Combine quantitative metrics and expert judgement to assess analogue suitability.

175 4. Estimate the f -M relationship for Melimoyu using eruption records from a selection of
176 analogues.

177 SERNAGEOMIN will use the set of analogues and the f -M relationship to inform the volcanic hazard
178 matrix and official hazard map for Melimoyu. Future work will explore the application of Melimoyu's
179 analogues for populating an event tree and identifying eruption source parameters for a probabilistic
180 long-term hazard assessment. The clustering results are also provided to SERNAGEOMIN so that the
181 suitability of different potential analogues can be assessed for other data-limited volcanoes in Chile.

182 **2. Geological setting**

183 Melimoyu is a 2408 m high ice-capped composite volcano with a 1-km wide crater summit and several
184 parasitic cinder cones (GVP, 2013). The characteristic oblique subduction in the Chile Triple Junction,
185 crustal thickness, and Liquiñe-Ofqui Fault Zone (LOFZ) (Fig. 1a) are responsible for the variable nature
186 of the volcanism, volcanic forms, and rock composition in this area (Cembrano and Lara, 2009; de
187 Pascale et al., 2021; Völker et al., 2011). The LOFZ intra-arc fault system also controls the spatial
188 distribution and the type of volcanism of the southern segment of the Southern Volcanic Zone (SVZ),
189 from Villarrica in the north to Hudson in the south, with contrasting eruptive styles between volcanoes
190 on the compressive side with wide ranges of compositions and volcanoes on the extensive side with
191 more primitive magmas (Cembrano and Lara, 2009; de Pascale et al., 2021; Gutiérrez et al., 2005;
192 López Escobar et al., 1995; Stern et al., 2007). The paleo-seismic Holocene record in the Aysén region
193 shows that the triggering of several Holocene volcanic eruptions could be closely linked to earthquakes
194 from the LOFZ and megathrust earthquakes (Watt et al., 2009; Wils et al., 2018).



195

196 **Fig. 1.** Map of the Southern Volcanic Zone (SVZ) (33°S-46°S) a) and surroundings of Melimoyu b).
 197 Holocene volcanoes from the VOTW database are marked with black triangles, Melimoyu is marked
 198 with a yellow triangle in a) and with a black triangle in b), analogues of Melimoyu in the SVZ are
 199 marked with a red triangle. Aysén region is highlighted in dark grey. Plate boundaries extracted from
 200 Bird (2003), and active and potentially active faults from the Liqueñe-Ofqui Fault Zone (LOFZ)
 201 extracted from Melnick et al. (2020) are represented with black lines. Basemap a) ESRI Shaded Relief,
 202 b) ALOS PALSAR DEM 12.5 m resolution.

203 The nearest towns of La Junta (1431 inhabitants; Instituto Nacional de Estadísticas (2019)) and Puerto
 204 Raúl Marín Balmaceda (239 inhabitants; Instituto Nacional de Estadísticas (2019)) are located around
 205 40 km to the east and 33 km to the northwest from the volcano (Fig. 1b), respectively, in the sparsely
 206 populated region of Aysén (e.g., total population of 103,158 according to the last census from 2017
 207 (Instituto Nacional de Estadísticas, 2019)). Tephra fall deposits are found around these localities,
 208 suggesting that future eruptions could affect the population in this area and disrupt the Carretera Austral
 209 (Naranjo and Stern, 2004), which is the only road access to Aysén region (Rojas Hoppe and Subiabre,
 210 1998). The little village of Villa Melimoyu, with around 100 inhabitants (Instituto Nacional de
 211 Estadísticas, 2019), located at Marchant River valley around 19 km southwest of the volcano, could

212 also be affected by PDCs or lahars, given the explosive nature of Melimoyu (Geoffroy et al., 2018;
213 Naranjo and Stern, 2004) and the size of the glaciers in the volcanic edifice (Daros Idalino et al., 2020).

214 The Holocene record from Melimoyu contains two confirmed eruptions: i) Mm-1 dated around 2.8ka
215 BP, and ii) Mm-2 dated around 1.6ka BP (Geoffroy et al., 2018; Naranjo and Stern, 2004). Geoffroy et
216 al. (2018) reported that the column height for Mm-1 and Mm-2 ranged between ~30-35 km and ~26-30
217 km, respectively, establishing that both eruptions had a VEI 5. In addition, several tephra layers found
218 in lakes and rivers in the area, which dated ~4.6-4.8 ka BP, ~8.3 ka BP, and before the Last Glacial
219 Maximum at >19,670 BP, have been attributed to Melimoyu due to similarities in the geochemistry,
220 although their origin and size have not been confirmed (Stern et al., 2015; Weller et al., 2017).

221 **3. Data**

222 *3.1 Global database*

223 The global database (supplementary material 1) includes 1428 volcanoes categorised as Holocene in
224 the VOTW database (v. 4.8.5; 11 February 2020) (GVP, 2013). We excluded 31 volcanoes from the
225 analysis because they were discontinued from the GVP Holocene Volcano List as of August 2021. Our
226 database contains 181 variables describing general information from each volcano and its Holocene
227 eruption record, rock composition, tectonic setting, and morphology.

228 **General information (53 variables)**

229 General information about each volcano and its Holocene eruptive history was obtained from the
230 VOTW database (GVP, 2013). We included categorical variables describing the tectonic setting,
231 morphology, and rock composition, the volcano location, date of the most recent eruption, range of VEI
232 in the Holocene, number of eruptions as a function of VEI, and number of hazards and processes (i.e.,
233 events in GVP terminology).

234 **Rock composition (17 variables)**

235 The composition was compiled from the VOTW database (GVP, 2013) and the EarthChem Portal
236 (<http://www.earthchem.org>, downloaded on 31 October 2022, using the parameters: Volcano Name =
237 All volcanoes, Age = Holocene (0 Ma – 0.01 Ma), Material= Whole rock/rock, and normalization=
238 Major Elements as Reported). The GVP lists a maximum of five rock types for each volcano, which
239 were extracted by scraping the profiles from their website. Siebert et al. (2015) classified the
240 composition into ten rock types: Andesite/Basaltic Andesite, Basalt/Picro-Basalt, Dacite, Foidite,
241 Phono-tephrite/Tephri-phonolite, Phonolite, Rhyolite, Trachyandesite/Basaltic Trachyandesite,
242 Trachybasalt/Tephrite Basanite, and Trachyte/Trachydacite.

243 Since the rock types in the GVP are listed in descending order of abundance (Siebert et al., 2015), we
244 assumed that rock type 1 is five times more abundant than rock type 5 and assigned a weight ranging
245 from five to one to each of the up to five rock types. We normalised the weights considering the number
246 of rock types available per volcano and assigned them to each rock type. For example, West Eifel
247 Volcanic Field (Germany) has the following rock types listed in order of descending abundance:
248 Foidite, Trachybasalt/Tephrite Basanite, and Phonolite. Since there are three out of five possible rock
249 types, we add 5, 4, and 3 to a total weight of 12. Then, we assigned 5/12 to Foidite, 4/12 to
250 Trachybasalt/Tephrite Basanite, 3/12 to Phonolite, and zero to the remaining rock types not listed in the
251 West Eifel Volcanic Field GVP profile. With this approach, we captured the range of compositions and
252 the relative abundance.

253 From the dataset downloaded from EarthChem Portal, we filtered the igneous and volcanic samples and
254 extracted the SiO₂ wt%, from which we calculated the minimum, maximum, median, mean, mode,
255 standard deviation, and variance across all the available samples per volcano. One limitation we found
256 when downloading data from multiple volcanoes from the EarthChem portal is that the volcano name
257 is not associated with the sample name. Therefore, we used the linear distance matrix tool from QGIS
258 (N*K*3) to assign each sample to the nearest volcano. As a result, we have 2090 samples distributed
259 across 125 volcanoes. The number of samples per volcano ranges from 1 for each of 34 volcanoes to
260 281 for Vesuvius.

261 **Tectonic setting (44 variables)**

262 One of the variables compiled for the tectonic setting is the total crustal thickness (excluding the water
263 layer) extracted from the Global Model of Earth's Crust CRUST1 (Laske et al., 2013). We used the
264 distance matrix tool in QGIS to identify the nearest data point (pair of coordinates set at 1 degree) from
265 each volcano.

266 We also calculated the distance to the closest plate boundary classes (i.e., oceanic spreading ridge
267 (OSR), oceanic transform fault (OTF), oceanic convergent boundary (OCB), continental rift boundary
268 (CRB), continental transform fault (CTF), continental convergent boundary (CCB), and subduction
269 zone (SUB)) from each volcano (Bird, 2003). We used the midpoints of each digitisation step (end point
270 of PB2002.dat in Bird (2003)) as the reference point to calculate the distance. We also extracted the
271 plate boundary identifier and the plate boundary class for the closest boundary class.

272 For volcanoes in subduction zones, we extracted 17 variables from Heuret (2006) describing the relative
273 and absolute movement of plates at the nearest subduction arc segment (e.g., normal component of the
274 subducting velocity), the age of the slab and the thermal parameter. The study by Heuret (2006) only
275 includes non-perturbed subduction zones, which are those distant from a collision zone, ridge, or plateau

276 subduction. Additionally, we used the same arc segment names from Heuret (2006) to extract the
277 variables slab length, slab pull force, Upper Plate Strain (UPS), and Upper Plate Nature (UPN) from
278 Lallemand et al. (2005).

279 Lastly, we extracted the depth, dip, strike, and thickness of the slab at each subduction zone volcano
280 from the Slab2 model developed by Hayes et al. (2018), which is available in the USGS ScienceBase
281 catalogue (Hayes, 2018).

282 **Morphology (64 variables)**

283 To describe the morphology, we used the database from Grosse et al. (2014) and Grosse and Kervyn
284 (2018), which characterises the morphometry of composite, calderas, and shield volcanoes. The
285 variables included in these databases describe the edifice size, profile shape, plan shape, and slope
286 (Grosse et al., 2014). We updated the values in Grosse et al. (2014) with those from Grosse and Kervyn
287 (2018) for volcanoes included in both studies. Seventeen of the 64 variables compiled from these studies
288 are only available for calderas or composite volcanoes with large summit craters.

289 *3.2 Input dataset*

290 The input dataset for the clustering contains only volcanoes with data for all the selected variables since
291 we do not allow missing values in the clustering. In addition, we only considered numerical variables
292 in the analysis, excluding 16 categorical variables, three textual variables, and 13 identifiers. We also
293 excluded ten uninformative variables, such as the number of elevation contours in Grosse et al. (2014).
294 As discussed in the introduction, we want to avoid clustering volcanoes based on their degree of
295 completeness, which, in the case of Melimoyu, would presumably produce analogues that are also data-
296 limited volcanoes. Therefore, we excluded 36 variables related to eruptive history or style. We also
297 excluded coordinates since we want to avoid grouping volcanoes by their proximity ($n=4$). Lastly, since
298 our application of AGNES is targeted at Melimoyu, we excluded 31 variables with missing data for
299 Melimoyu, among which we have the eight variables calculated from the data extracted from
300 EarthChem.

301 The remaining variables are considered of interest for our case study. Since we do not allow missing
302 data in the clustering and most tectonic setting variables describe characteristics of subduction zones,
303 we automatically exclude volcanoes from other tectonic settings. Therefore, we only retain the distance
304 to the nearest plate boundary (i.e., subduction zone) and exclude the other seven variables that measure
305 the distance to different plate boundary types. Lastly, for variables accounting for duplicated
306 information (e.g., edifice height, basal width, and height/basal width ratio from Grosse et al. (2014)),

307 we preferentially selected variables not calculated as a function of other variables in the database,
308 leading us to exclude 22 variables.

309 As a result of this filtering, we have 38 numerical variables (10 for rock composition, 14 for tectonic
310 setting, and 14 for morphology) available for 438 subduction zone volcanoes. Note that Foidite is not
311 included in the clustering because none of these volcanoes has records of this rock type in the VOTW
312 database. The input dataset for Melimoyu can be accessed in supplementary material 2, and the
313 complete list of 37 variables after excluding Foidite is listed in Table 1 and Figure 3.

314 **4. Methodology**

315 *4.1 Hierarchical clustering*

316 In this study, we used AGNES, a bottom-up hierarchical clustering approach (Kaufman and Rousseeuw,
317 1991). The main advantage of hierarchical clustering is that it does not require the number of clusters
318 to be pre-defined. We selected agglomerative instead of divisive hierarchical clustering because the
319 former tends to identify smaller clusters (Boehmke and Greenwell, 2019). Before applying AGNES,
320 we calculated the (dis)similarity matrix, which contains the distance among pairs of volcanoes. We
321 selected the Manhattan distance metric because it performs better than the Euclidean distance for high-
322 dimensional datasets (Aggarwal et al., 2001), and is less sensitive to outliers (Strauss and Von Maltitz,
323 2017).

324 In AGNES, each observation (volcano) starts as a single cluster (leaf). Then, based on the Manhattan
325 distance, the most similar pair of volcanoes are grouped into a bigger cluster (node or branch). Lastly,
326 the most similar clusters are merged iteratively until all the volcanoes are grouped into one big cluster
327 (root). The (dis)similarity between clusters is determined by the linkage method. Some commonly used
328 methods are average linkage, single linkage, complete linkage, and Ward's linkage (we refer the reader
329 to Kaufman and Rousseeuw (1991) for more details on each method). To select the best linkage method,
330 we ran AGNES using these four methods and retained the results that produced the highest
331 agglomerative coefficient – Ward's linkage. The agglomerative coefficient describes the strength of the
332 clustering structure, with values closer to 1 indicating a strong clustering structure (Kaufman and
333 Rousseeuw, 1991).

334 The agglomerative coefficient can be considered a form of internal validation of the clustering since it
335 measures the quality of the clustering structure without reference to external information (Boehmke and
336 Greenwell, 2019). Another form of internal validation is assessing the clustering tendency of the input
337 data (Banerjee and Davé, 2004). The clustering tendency evaluates if the dataset contains an inherent
338 grouping structure. One metric used to assess the clustering tendency is the Hopkins statistic (H), which
339 estimates the probability that the dataset is generated by a random uniform distribution (Lawson and

340 Jurs, 1990). The input data are highly clusterable when H is close to 1. We used the agglomerative
341 coefficient and Hopkins statistic metrics to compare the quality of the clustering results from the
342 sensitivity analysis.

343 The output of AGNES is a dendrogram, a tree-based representation containing leaves, nodes, and the
344 root. The height of the dendrogram (horizontal axis in Figures 2, 5, and 6) represents the distance (i.e.,
345 (dis)similarity) between clusters. Note that the height values are not comparable between the
346 dendrograms presented in this study because they are constructed using different input data. Therefore,
347 the height can only be used to interpret the similarity between clusters within their dendrogram. The
348 height at which we cut the dendrogram controls the number of clusters generated. Instead of searching
349 for the optimal number of clusters, which is the main challenge when using other clustering algorithms,
350 we found the height that generates a cluster of at least 50 potential analogues for Melimoyu. In this
351 study, we want to avoid retaining larger numbers of potential analogues so the suitability assessment of
352 individual volcanoes is not excessively time-consuming. Thanks to the flexibility of AGNES, future
353 applications can adjust the number of analogues to fit their goal.

354 To compare the similarity between Melimoyu and the potential analogues, we normalised the
355 Manhattan distance (M_{norm}) via min-max normalisation as follows:

$$356 \quad M_{norm} = 1 - \frac{M - M_{min}}{M_{max} - M_{min}} \quad (1),$$

357 where the maximum, M_{max} , and minimum value, M_{min} , corresponds to the highest and lowest Manhattan
358 distance, respectively, within the set of potential analogues, including Melimoyu (i.e., M_{norm} ranges from
359 0 for the least similar volcano to 1 for Melimoyu).

360 *4.2 Sensitivity analysis*

361 We performed a sensitivity analysis on three different input datasets to assess how they change the
362 outcome of the clustering, which are the proposed analogue volcanoes, and the quality of the results in
363 terms of internal validation metrics.

364 **Raw dataset**

365 The first application of AGNES was made on the selection of 37 variables. Each variable was
366 standardised (i.e., centred and scaled) so that the distribution of the transformed data, known as z-score,
367 had a mean of 0 and a standard deviation of 1 (Han et al., 2012). Standardising the data is an essential
368 pre-processing step when using machine learning models on data measured with different units,
369 covering wide ranges of values, or in the presence of outliers since it has been shown to improve the
370 quality of the clustering (Mohamad and Usman, 2013).

371

372 **Reduced dataset**

373 The preparation of the second input dataset consisted of two steps aimed at capturing the most important
374 variables by excluding redundant variables and reducing noise in the data.

375 Firstly, we removed five redundant variables from the original dataset of 37 variables and standardised
376 the dataset. The redundant variables were identified from the correlation between variables. As almost
377 all the variables are non-normally distributed, we used Kendall's Tau correlation coefficient (Chen and
378 Popovich, 2002). Lastly, we classified the strength of the correlation as very weak ($0 < r < 0.2$), weak
379 ($0.2 \leq r < 0.4$), moderate ($0.4 \leq r < 0.6$), strong ($0.6 \leq r < 0.8$), and very strong ($0.8 \leq r < 1$). We used $r \geq 0.8$ as the
380 threshold to identify which redundant variables should be excluded from the Principal Component
381 Analysis (PCA) so that there are no pairs of very strongly correlated variables in the input data. We
382 remove the variable with the largest mean absolute correlation for very strongly correlated variables.
383 Although PCA can handle redundant variables, we preferred to include this step to ensure that all
384 detrimental redundancies were removed from the dataset.

385 Secondly, we applied a PCA to the dataset derived from the first. This approach is used to deal with the
386 'curse of dimensionality' before using clustering algorithms (Assent, 2012) by transforming the original
387 variables into uncorrelated Principal Components (PC) through linear combination (Abdi and Williams,
388 2010). The PCA helps to improve the interpretability of high-dimensional datasets by reducing the
389 dimensions and capturing the maximum possible variance of the original data. The number of PCs to
390 retain for the analysis is often based on an arbitrary percentage of the cumulative variance. In this study,
391 we used a threshold of 70% since it is a commonly used value (Jolliffe and Cadima, 2016), although
392 other thresholds could be tested to assess the influence of the variance of the input data on the clustering.
393 The coordinates or scores from each volcano in the retained PCs were used as input data for the
394 clustering.

395 **Weighted dataset**

396 For the third dataset, we applied a weighting scheme on the raw dataset (i.e., 37 standardised variables)
397 tuned to minimise the dispersion of the absolute probability from the set of potential analogues. With
398 this approach, we acknowledge that each variable is unlikely to have equal influence on the clustering
399 of volcanoes with analogous eruptive behaviour (i.e., similar f - M relationship).

400 The steps we followed were:

- 401 1. Draw a set of 37 weights from a uniform distribution and normalise so all weights add to one.
- 402 2. Apply AGNES using the best linkage method identified from the raw and reduced dataset
403 (Ward's linkage) with variables weights from step 1.
- 404 3. Extract a set of at least 50 potential analogues.

- 405 4. Estimate the absolute probability per VEI (i.e., the annual probability of an eruption of a given
 406 VEI) (P_{ABS}) for each analogue volcano i :

407
$$P_{ABS\ ij} = \frac{n_{ij}}{t_{ij}} \quad (2),$$

408 where n_{ij} is the number of recorded eruptions of a given VEI j (VEI ≤ 1 , VEI 2, VEI 3, VEI 4,
 409 and VEI ≥ 5) and t_{ij} is the number of years between the Relative Completeness Date (RCD) and
 410 2019. We calculate the regional RCDs (i.e., the most complete portion of the catalogue) from
 411 the VOTW database (GVP, 2013) as a function of each VEI j using the most abrupt change
 412 point method from Burgos et al. (2022b) and the 31 new regions proposed in their study
 413 (supplementary material 3).

- 414 5. Calculate the Interquartile Range (IQR_j) of the absolute probability per VEI for the set of
 415 potential analogues, which captures the spread of the data between the 25th and 75th percentile.
 416 6. Calculate the total IQR by adding all IQR_j .
 417 7. Optimise 10,000 vectors of weights to identify the set of weights that minimises the total IQR.

418 When the target volcano is well-studied and has comprehensive records, this approach can be modified
 419 to identify the weights that maximise the similarity of the analogues' absolute probabilities to the target
 420 volcano. We discarded this option for Melimoyu because it only has data to calculate the absolute
 421 probability of VEI 5 eruptions, meaning that we would be aiming to find other data-limited volcanoes.

422 4.3 Analogue selection

423 The selection of analogues was made by assessing the dispersion in the absolute probability derived
 424 from the potential analogues (Fig. 7) and applying criteria deemed as important by SERNAGEOMIN
 425 and VB to estimate the f -M relationship for Melimoyu. A particular volcano had to meet the following
 426 criteria to be considered an analogue of Melimoyu:

- 427 a) The volcano has confirmed Holocene eruptions with an assigned VEI in the VOTW (GVP,
 428 2013) or LaMEVE database (Crosweller et al., 2012). Otherwise, the eruptive behaviour cannot
 429 be evaluated.
 430 b) The volcano is not categorised as frequently active (i.e., “confirmed to have erupted at some
 431 point during at least 25 of the past 100 years (since 1921)” (GVP, 2013)) on the set of
 432 noteworthy volcanoes of the GVP
 433 (https://volcano.si.edu/faq/index.cfm?question=eov_noteworthy). This criterion is especially
 434 relevant for estimating the f -M relationship for Melimoyu since there is no evidence of
 435 eruptions in the last 100 years. With this criterion, we may be excluding analogue volcanoes
 436 that can be used for other purposes (e.g., retrieving eruption source parameters for hazard
 437 modelling).

- 438 c) The volcano has records of large explosive Holocene eruptions ($VEI \geq 4$) in the VOTW (GVP,
 439 2013) or LaMEVE database (Crosweller et al., 2012).
- 440 d) The volcano has produced similar compositions to Melimoyu in the past. The GVP lists, in
 441 order of descending abundance, the following rock types for Melimoyu: Andesite/Basaltic
 442 Andesite, Dacite, and Basalt/ Picro-Basalt. Depending on the information available in the GVP,
 443 if the volcano has data for:
- 444 • *Rock types 1, 2 and 3*: it must have at least two rock types in common with Melimoyu,
 445 and the most abundant rock type must be intermediate or felsic.
 - 446 • *Rock types 1 and 2*: it must have both rock types in common with Melimoyu,
 447 independently of the order, but the most abundant rock type must be intermediate or
 448 felsic.
 - 449 • *Rock type 1*: it must be Andesite/Basaltic Andesite.

450 4.4 Frequency-magnitude relationship

451 Once we had the selection of analogues for Melimoyu, we manually updated the start date for those
 452 large magnitude eruptions ($M \geq 4$) that had corrected dates in the latest version of LaMEVE (retrieved
 453 17 August 2022) (Crosweller et al., 2012). We also included $M \geq 4$ Holocene eruptions that were missing
 454 in the VOTW database but available in the LaMEVE database.

455 The updated record of confirmed eruptions since the RCDs from the selection of analogue volcanoes
 456 was used to re-calculate the absolute probability per VEI (P_{ABS}). The sum of the absolute probabilities
 457 per VEI from each analogue gives us the absolute probability of having an eruption of any VEI (P) at a
 458 given analogue volcano i :

$$459 \quad P_i = \sum_k P_{ABS\ ik} \quad (3)$$

460 Using the absolute probability, we calculated the conditional probability P_{COND} (i.e., the relative
 461 probability of a given VEI j , conditional on an eruption occurring) per analogue volcano i as follows:

$$462 \quad P_{COND\ ij} = \frac{P_{ABS\ ij}}{\sum_k P_{ABS\ ik}} \quad (4),$$

464 where k indicates the VEI j with a $P_{ABS\ ij} \neq 0$.

465 The absolute and conditional probabilities from the set of analogues were used to estimate the f - M
 466 relationship for Melimoyu as follows:

- 467 1. Model the empirical absolute probability P from the set of analogues by a Gamma
 468 distribution, as proposed by Rodado et al. (2011) and Solow (2001), with parameters α

469 (shape) >0 and λ (rate) >0 estimated via maximum likelihood. The probability density
 470 function of a gamma distribution is given by:

$$471 \quad f(x) = \begin{cases} \frac{\lambda x^{\alpha-1} e^{-\lambda x}}{\Gamma(\alpha)}, & x > 0 \\ 0, & x \leq 0 \end{cases} \quad (5)$$

472 We extract the 5th, 50th, and 95th percentiles from the Cumulative Distribution Function
 473 (CDF), which reflects the uncertainty in the absolute probability for Melimoyu.

474 2. Quantify the variability in the conditional probability P_{COND} via bootstrapping with
 475 replacement (i.e., a datapoint can be included more than once in a resampled dataset). From
 476 the empirical conditional probabilities for n analogue volcanoes calculated from eq. 4, we
 477 draw 5,000 bootstrap samples of size n and calculate the average conditional probability
 478 per VEI from each resampled dataset. We extract the 5th, 50th, and 95th percentiles from the
 479 marginal empirical CDF of the conditional probability for each VEI.

480 3. Calculate the absolute probability per VEI j for Melimoyu as follows:

$$481 \quad P_{ABSj} = P \times P_{CONDj}$$

482 5. Results

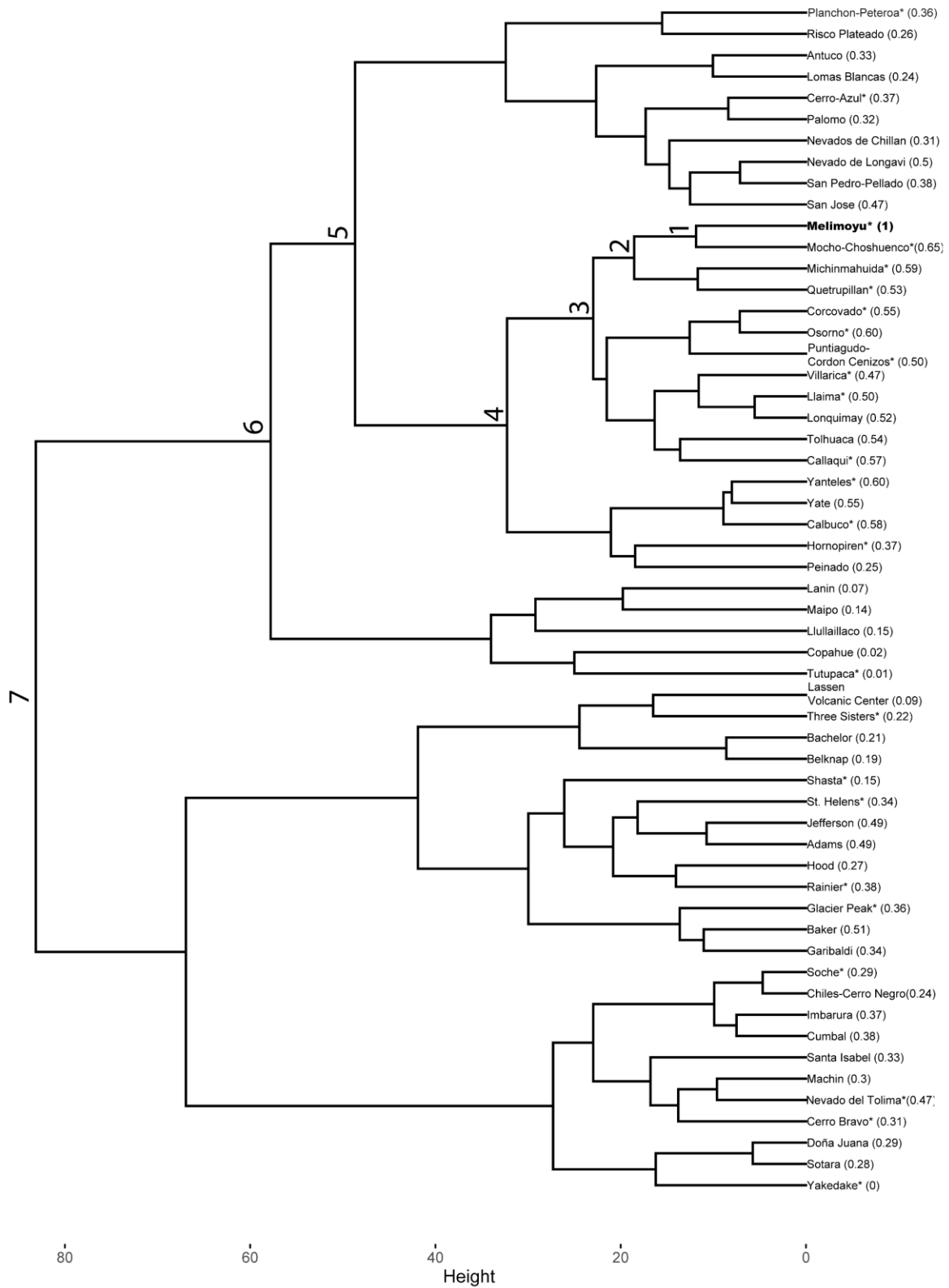
483 5.1 Analogues from the raw dataset

484 The agglomerative coefficient of the hierarchical clustering ranges from 0.778 for the single linkage
 485 method to 0.949 for Ward's linkage method, indicating that the latter is the best linkage method. The
 486 agglomerative coefficient close to 1 indicates a strong clustering structure in the dendrogram derived
 487 from the raw dataset. This indication of good quality of the clustering is corroborated by the Hopkins
 488 statistics (H) of 0.848, which indicates that the raw dataset is highly clusterable.

489 We cut the dendrogram at the minimum height that contains at least 50 volcanoes, approximately 80,
 490 generating a set of 56 potential analogues, including Melimoyu (Fig. 2). Within this set of potential
 491 analogues, we find seven nodes connected to Melimoyu's smaller cluster (Node 1), which indicate
 492 different levels of similarity (i.e., the higher up in the tree the least similar to Node 1). Forty-two
 493 potential analogues are in the region of South America, 13 in Canada and Western USA, and 1 in
 494 Honshu (Japan).

495 Based on the normalised Manhattan distance shown in Figure 2 (i.e., the closer to 1, the more similar
 496 to Melimoyu), Mocho-Choshuenco (Chile) is the most similar volcano to Melimoyu ($M_{norm}=0.65$) and
 497 therefore, the best analogue when using this method. The dendrogram captures this similarity since it

498 is the first volcano to be grouped with Melimoyu. Osorno, Yanteles, Michinmahuida, Calbuco, and
 499 Callaqui, also located in Chile, follow closely with relatively similar distances.



500

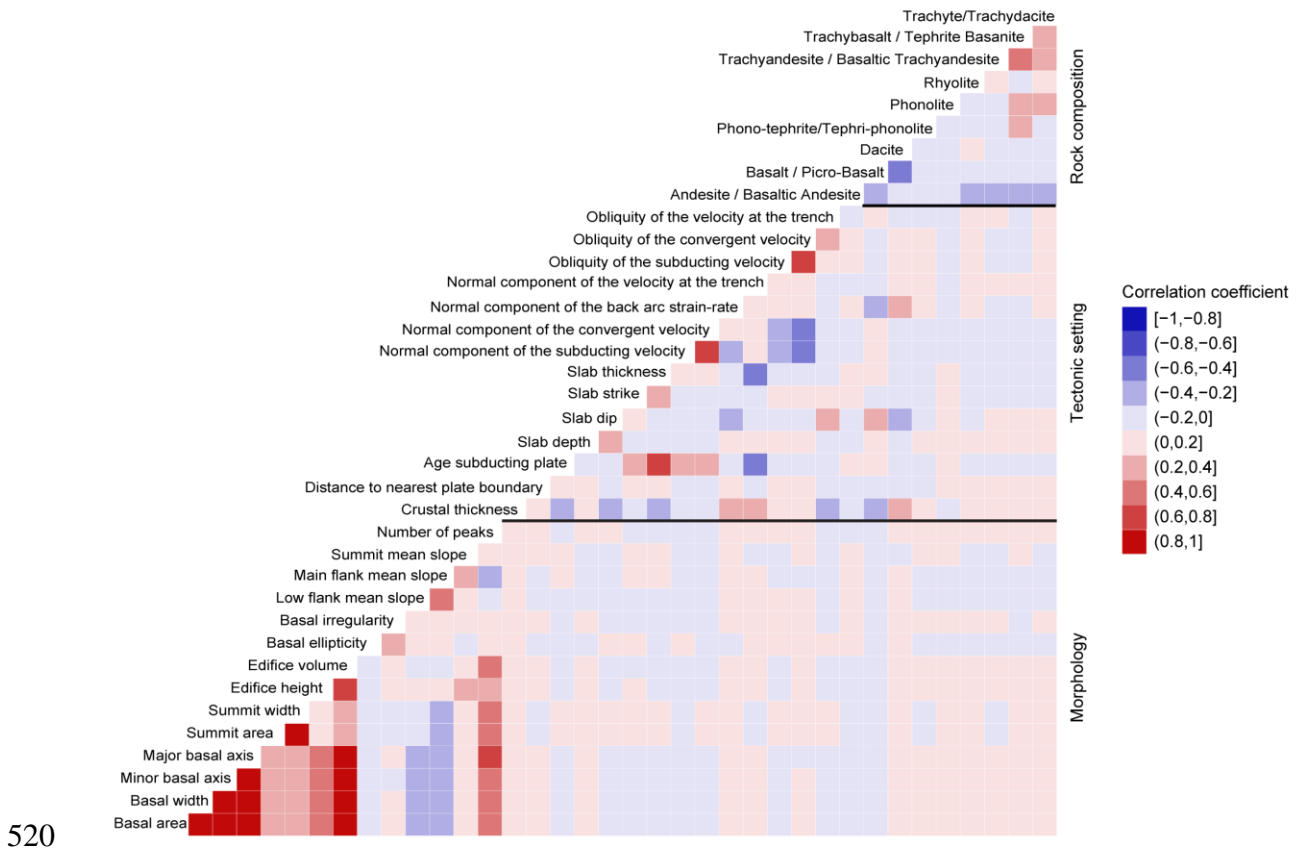
501 **Fig. 2.** Dendrogram generated from the application of AGNES using Ward's linkage method to the raw
502 dataset. The value in parenthesis shows the normalised Manhattan distance (M_{norm}). The closer M_{norm} is
503 to 1, the most similar to Melimoyu (highlighted in bold). The node number indicates the different levels
504 of similarity between a given cluster and the smaller cluster that contains Melimoyu (Node 1). The
505 asterisk indicates if a volcano has $\text{VEI} \geq 4$ Holocene eruptions records in the VOTW or LaMEVE
506 database.

507 *5.2 Analogues from the reduced dataset*

508 Using Kendall's Tau correlation coefficient to assess the relationship between the variables, the
509 correlation matrix shown in Figure 3 shows that several variables describing the morphology of the
510 base and the summit's edifice are very strongly correlated. Since we aim to exclude redundant variables
511 (i.e., $r \geq 0.8$), the following variables are not considered for the PCA: minor and major basal axis, basal
512 width, basal area, and summit width.

513 Other variables with a strong positive correlation are the age of the subducting plate and slab thickness,
514 normal convergent and subducting velocity components, and the convergent and subducting obliquity.
515 For the rock composition, we observe that Trachy-Andesite/Basaltic Trachyandesite and
516 Trachybasalt/Tephrite Basanite have a moderate positive correlation. In contrast, Basalt/Picro-Basalt
517 and Dacite have a moderate negative correlation. Basalt/Picro-Basalt and Dacite also show a weak
518 correlation with the crustal thickness, slab dip, and the normal component of the back arc strain-rate.

519



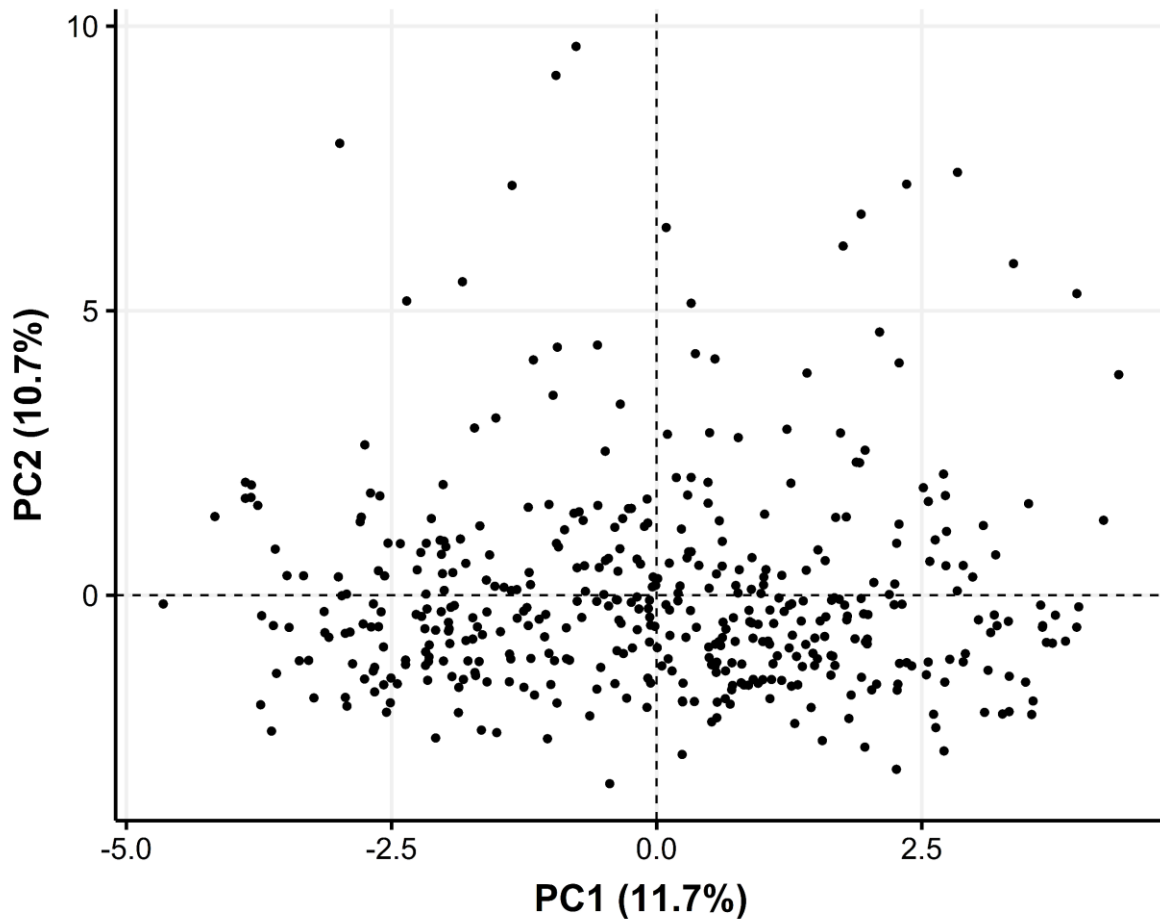
520

521 **Fig. 3.** Kendall's Tau correlation coefficient plot. Blue values indicate a negative correlation, and red
 522 values a positive correlation. The variables are grouped into three main categories: morphology,
 523 tectonic setting, and rock composition.

524 The standardised dataset of 32 variables (without redundant variables) was used as input for the PCA.
 525 The results of the PCA show that the first two components explain around 22% of the variance (Fig. 4).
 526 We require 11 PCs to capture at least 70% of the variance, which is one of the commonly used thresholds
 527 in PCA (Jolliffe and Cadima, 2016). Furthermore, the 11 PCs have an eigenvalue (i.e., variance retained
 528 by each PC) higher than one, indicating that they account for more variance than the original variables.
 529 The new spatial projection (Fig. 4) does not show any obvious spatial clusters of volcanoes, which can
 530 be due to the low variance retained by PC 1 and 2. A low variance in the main PCs could indicate that
 531 our dataset does not lie within a two-dimensional linear subspace. One solution we explored was using
 532 non-linear dimensionality reduction techniques (e.g., UMAP; (McInnes et al., 2020)). However, these
 533 techniques required tuning hyper-parameters by looking at how the data is distributed in the space,
 534 leading to a biased selection that could influence the clustering results.

535 Table 1 shows the percentage with which each variable contributes to explaining the variability in each
 536 PC (e.g., the age of the subducting plate explains ~17% of the variability in PC1). We observe that
 537 variables describing the tectonic setting (e.g., age of the subducting plate, slab thickness, normal
 538 component of the subducting velocity, crustal thickness, and obliquity of the subducting velocity)

539 contribute the most in accounting for the variability in PC1. In contrast, variables describing the volcano
 540 morphology (e.g., edifice volume, number of peaks, summit area, low flank mean slope, and main flank
 541 mean slope) have the highest contributions in PC2. Lastly, we observe that the composition contributes
 542 more to the later PCs.



543

544 **Fig. 4.** Representation of individual volcanoes projected in the PC1 and PC2. The value in parentheses
 545 indicates the percentage of explained variance by that PC.

546 **Table 1.** Variable contribution (%) of each variable to explain the variability for the 11 PCs retained
 547 for the analysis. The value in parentheses in the first row indicates the percentage of explained variance
 548 by that PC. Values in bold indicate the top 5 variables with the higher contribution to each PC. Variables
 549 are grouped by category and ordered by descending contribution in PC 1.

550

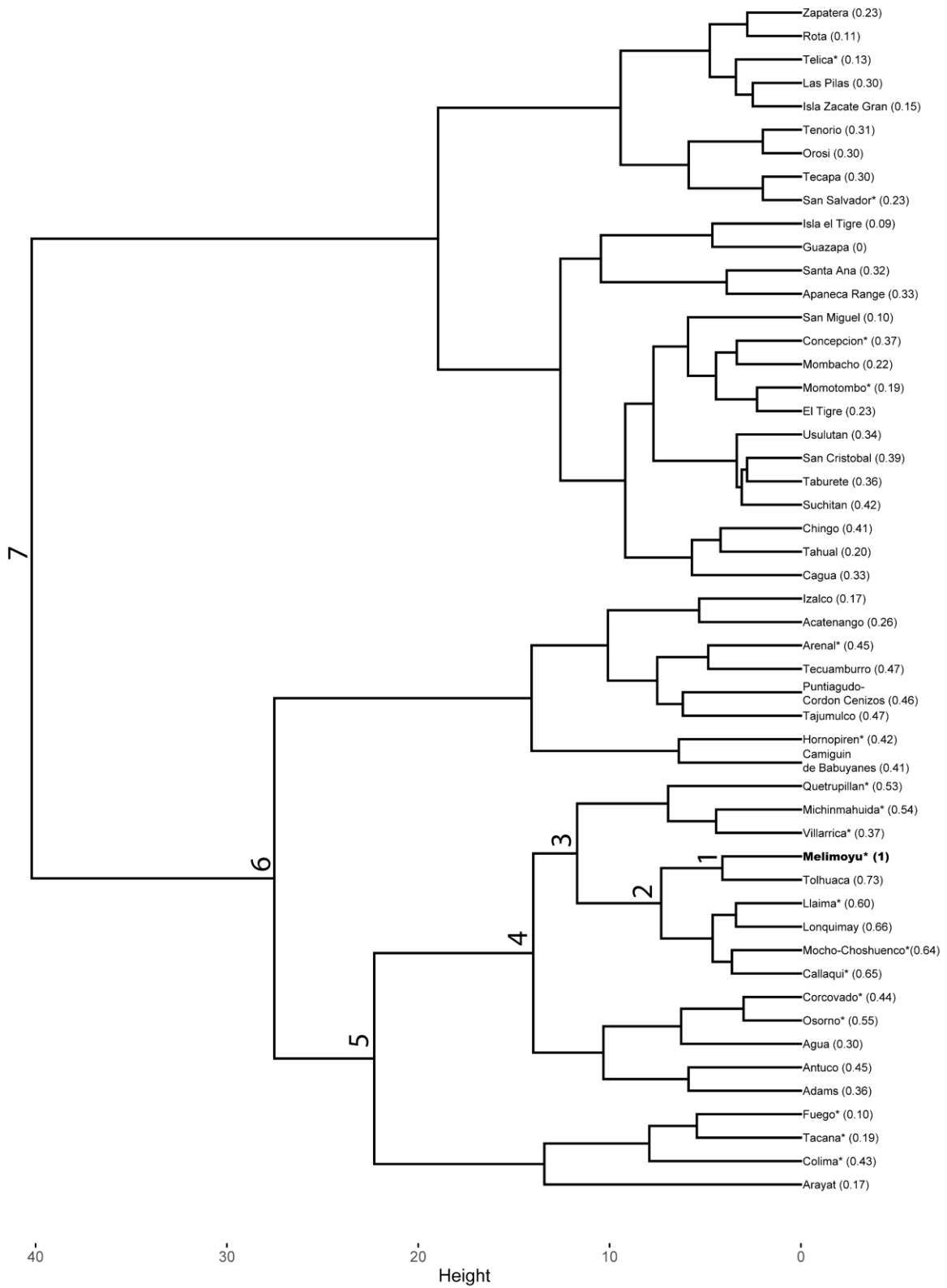
551

552

Variables	PC1 (11.7%)	PC2 (10.7%)	PC3 (8.9%)	PC4 (7.8%)	PC5 (6.2%)	PC6 (5.5%)	PC7 (4.8%)	PC8 (4.2%)	PC9 (3.9%)	PC10 (3.6%)	PC11 (3.5%)	
Tectonic setting	Age of the subducting plate	17.07	0.55	0.01	5.56	0.27	3.01	0.04	0.37	0.05	2.37	0.42
	Thickness of the slab	14.67	0.56	1.38	8.23	0.36	2.55	0.22	1.11	0.01	1.94	0.34
	Normal component of the subducting velocity	8.9	0.12	5.38	9.91	1.59	0.18	5.52	0.16	0.93	0	0.04
	Crustal thickness	7.85	0.13	11.03	0.9	0.53	2.62	1.83	0.39	0.02	0.65	0.07
	Obliquity of the subducting velocity	7.75	0.39	11.2	0.46	0.64	2.01	0.03	0.19	0.2	0.37	6.39
	Obliquity of the convergent velocity	7.1	0.31	16.09	0.15	1.46	1.28	0.9	0	0.07	0.05	1.1
	Normal component of the convergent velocity	5.1	0.47	14.22	0.83	0.56	0.74	3.01	0.11	0.02	0	0.55
	Normal component of the velocity at the trench	3.96	0.3	4.12	16.07	0.61	0.28	3.09	0	0.84	0.7	1.8
	Strike of the slab	3.41	0.6	1.86	3.99	1.32	0.73	1	3.43	2.46	3.74	0
	Normal component of the back arc strain-rate	1.7	0.13	1.02	7.97	5.62	1.43	21.17	0.03	1.24	0	1.31
	Obliquity of the velocity at the trench	1.08	0.01	12.34	1.42	0.25	4.69	0.05	0.05	1.63	0.17	2.55
	Dip of the slab	0.88	3.46	7.95	2.37	4.03	11.81	0.22	1.83	0.19	1.61	2.04
	Depth of the slab	0.13	6.6	0.06	0.23	5.49	0.54	1.49	11.86	1.58	0.11	1.21
	Distance to nearest plate boundary	0.02	0.55	0.26	8.23	2.1	4.1	1.7	0	2.7	4.78	0.21
	Rock composition	Basalt / Picro-Basalt	5.26	2.8	1.74	1.91	4.11	3.62	1.92	6.54	0.12	1.6
Rhyolite		0.69	0.11	0.06	0.07	0.01	0.16	2.01	1.02	8.29	19.8	31.81
Trachyte/Trachydacite		0.53	1.94	0.01	0.01	4.53	10.1	1.27	0.59	13.95	1.71	0.59
Phono-tephrite/Tephri-phonolite		0.31	0.29	0.05	0.01	1.91	1.73	5.38	2.64	39.67	1.96	5.81
Trachyandesite / Basaltic Trachyandesite		0.16	2.79	0.02	0	8.06	3.9	3	1.24	6.48	0.46	3.19
Andesite / Basaltic Andesite		0.12	5.77	0	1.5	7.33	1.74	1.02	6.47	1.69	30.59	2.43
Trachybasalt / Tephrite Basanite		0.07	5.11	0.07	0.17	8.7	7.34	9.46	0.14	10.49	0.29	1
Phonolite		0.03	1.01	0.01	0.62	3.69	2.78	1.52	10.04	1.8	1.25	5.17
Morphology	Basal irregularity	3.1	0.83	1.79	0	2.35	0.13	2.88	14.29	0.04	0.67	3.84
	Edifice height	1.81	1.24	2.87	8.52	0.01	6	8.96	3.59	1.62	0.05	0.05
	Low flank mean slope	0.82	10.16	1.19	0.28	2.41	3.5	4.1	1.51	0.02	4.45	8.49
	Number of peaks	0.56	13.2	0.55	2.33	3.93	3.21	0.17	3.93	0.35	1.23	0.3
	Edifice volume	0.48	13.39	1.14	4.68	4.62	4.44	4.03	0.02	0.03	0.42	1.04
	Summit mean slope	0.2	1.61	0.28	5.82	4.5	7.81	5.25	0.16	2.11	0.01	4.21
	Main flank mean slope	0.06	11.57	1.14	0.57	6.94	5.23	7.28	0.01	0.59	1.78	2.38
	Basal ellipticity	0.04	0.12	0	6.56	0.29	0.05	0.12	26.64	0.36	5.15	1.56
	Summit area	0.03	12.67	0	0.56	8.17	0.65	0.43	1.02	0.29	1.72	0.42

554 The reduced dataset containing the coordinates of 438 volcanoes at the 11 PCs was used as input data
555 for AGNES. The agglomerative coefficient ranges from 0.885 for single linkage method to 0.944 for
556 Ward's linkage method. As we did for the raw dataset, we select the hierarchical clustering results from
557 Ward's linkage method since it generates the strongest clustering structure. In addition, the Hopkins
558 statistic ($H=0.836$) indicates that the reduced dataset is highly clusterable.

559 We cut the resulting dendrogram (Fig. 5) at an approximate height of 40, producing a cluster of 51
560 volcanoes, including Melimoyu. This dendrogram contains groups of volcanoes with seven different
561 levels of similarity relative to the smaller cluster containing Melimoyu (Node 1). Twenty-one potential
562 analogues are in the region of Mexico, Guatemala, Nicaragua, Costa Rica, and Panama; 14 in South
563 America; 13 in El Salvador and Honduras; 2 in Luzon; 1 in North Luzon, Central Philippines,
564 Mindanao, and SE Asia; and 1 in Canada and Western USA. The volcano with the highest normalised
565 Manhattan distance (i.e., best analogue) ($M_{\text{norm}}=0.73$) is Tolhuaca (Chile). Other volcanoes with
566 relatively high distance values (e.g., $M_{\text{norm}}=0.60-0.66$) are Lonquimay, Callaqui, Mocho-Choshuenco,
567 and Llaima.



568

569 **Fig. 5.** Cut dendrogram generated from the application of AGNES using Ward's linkage method to the
 570 reduced dataset. The value in parenthesis shows the normalised Manhattan distance (M_{norm}). The closer

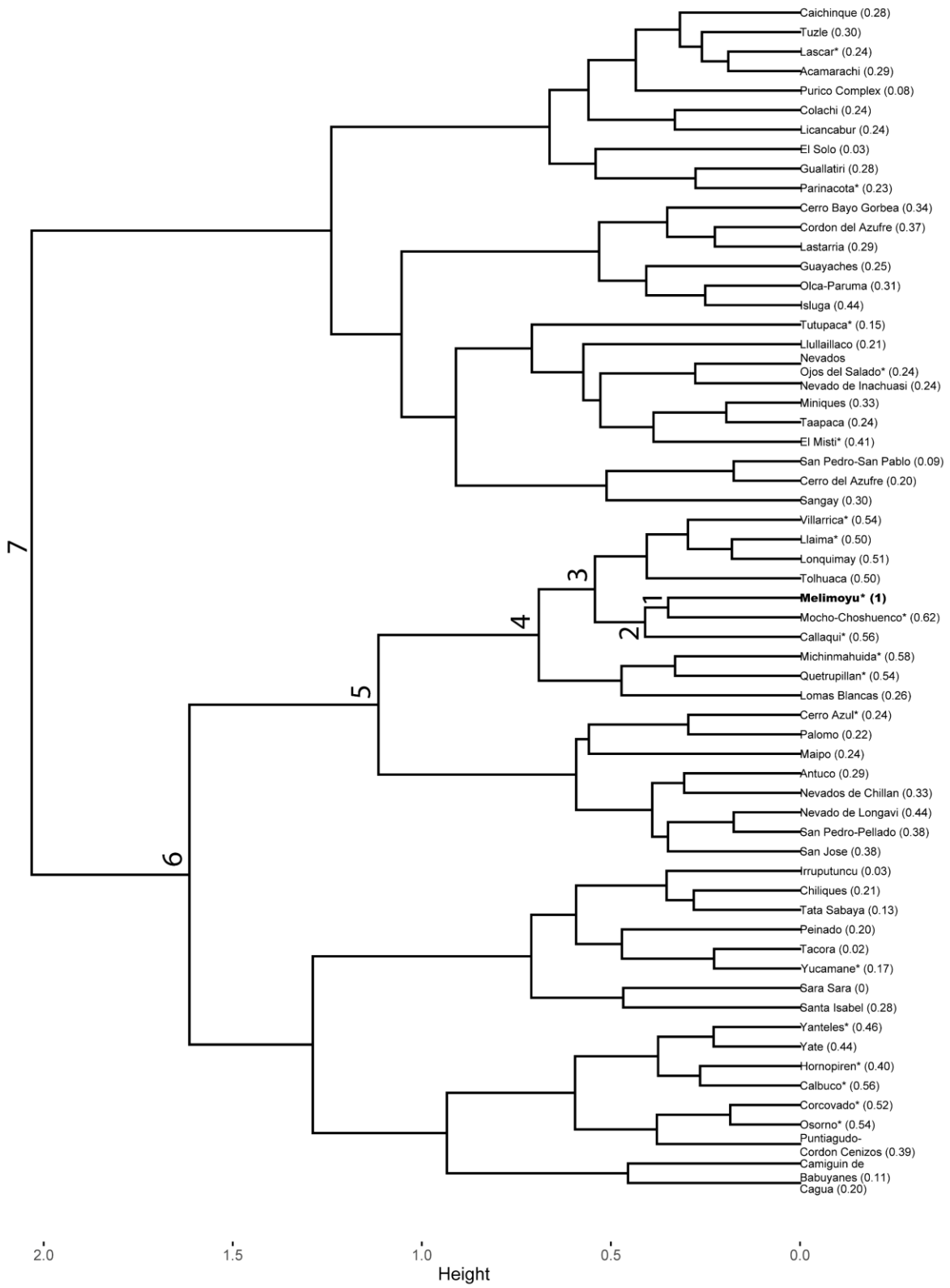
571 M_{norm} is to 1, the most similar to Melimoyu (highlighted in bold). The node number indicates the
572 different levels of similarity between a given cluster and the smaller cluster that contains Melimoyu
573 (Node 1). The asterisk indicates if a volcano has $\text{VEI} \geq 4$ Holocene eruptions records in the VOTW or
574 LaMEVE database.

575 *5.3 Analogues from the weighted dataset*

576 To optimize the set of weights that minimise the spread in calculated absolute eruption probabilities
577 across the set of analogues, we first need to account for the completeness of the eruption record. The
578 most complete portion of the VOTW database was identified by calculating regional RCDs as a function
579 of $\text{VEI} \leq 1, 2, 3, 4,$ and ≥ 5 using the change point method from Burgos et al. (2022b). The RCDs
580 (supplementary material 3) define the time windows required for absolute probabilities for the set of
581 potential analogues. The resulting RCDs range from a few centuries (e.g., 1979 for VEI 3 eruptions in
582 Africa (northern, western, central)) to thousands of years (e.g., 4700 BCE for VEI 4 eruptions in New
583 Zealand), and they are highly variable across regions and eruption sizes.

584 We use Ward's linkage method, which produced the highest agglomerative coefficients in the previous
585 two datasets, instead of testing the four linkage methods to reduce the computation time in optimising
586 the weighting scheme. The complete set of weights that generates the set of analogues with the lowest
587 total IQR (0.01214) is available in supplementary material 4. Another 11 weighting schemes that can
588 also be found in supplementary material 4 produce similar IQR (0.1224). We will focus on the results
589 derived from the weighting scheme that produces the lowest IQR. We observe that the three most
590 'important' variables (i.e., top 3 highest weights) are the obliquity of the velocity at the trench, the basal
591 irregularity, and the normal component of the convergent velocity.

592 The dendrogram obtained from the weighted dataset has an agglomerative coefficient of 0.947 and a
593 Hopkins statistic of 0.833, indicating a strong clustering. We cut the dendrogram at an approximate
594 height of 2 generating a set of 61 volcanoes, including Melimoyu (Fig. 6). We find seven levels of
595 similarity relative to the smaller cluster containing Melimoyu (Node 1). Fifty-nine potential analogues
596 are in the region of South America; 1 in Luzon; and 1 in North Luzon, Central Philippines, Mindanao,
597 and SE Asia. The most similar volcano based on the normalised distance metric is Mocho-Choshuenco
598 ($M_{\text{norm}} = 0.62$). Other similar volcanoes are Michinmahuida, Callaqui, Calbuco, and Osorno, with a
599 normalised distance ranging from 0.54 to 0.58.



600

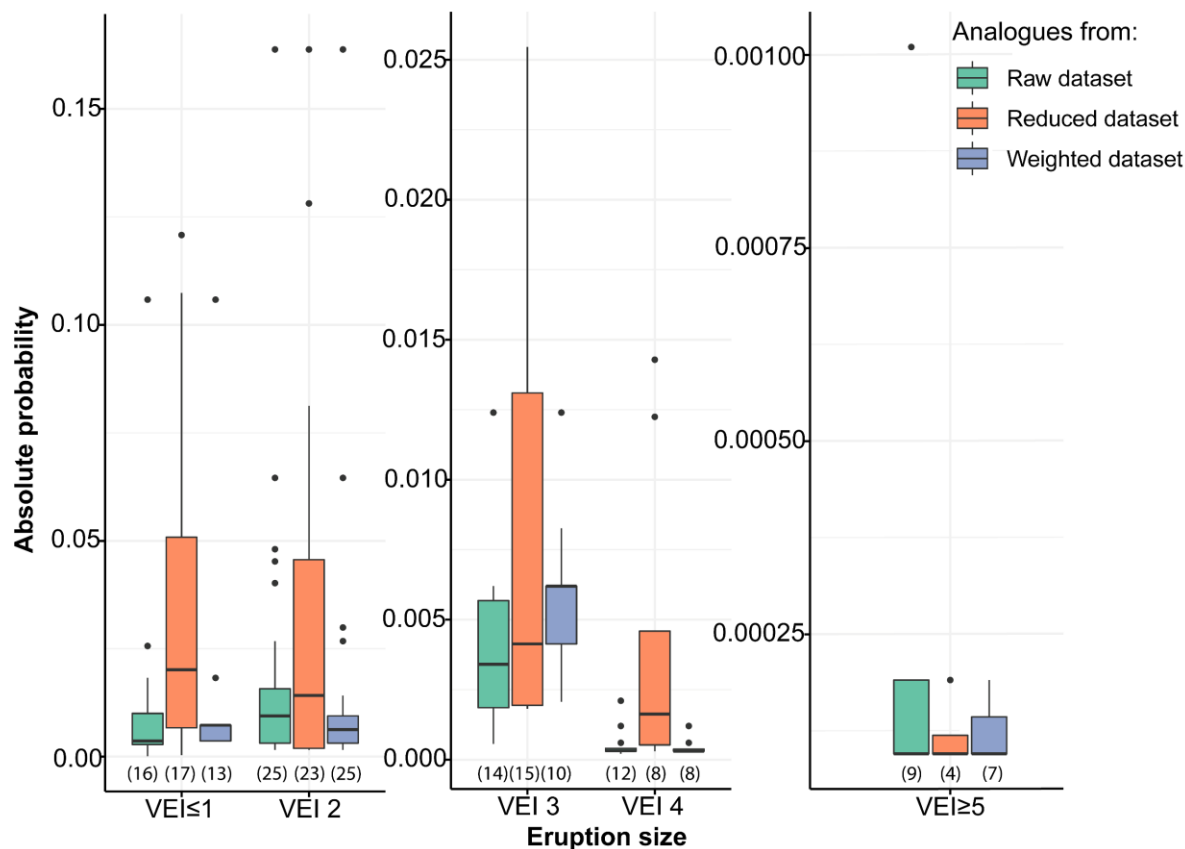
601

602 **Fig. 6.** Cut dendrogram generated from the application of AGNES using Ward's linkage method to the
603 weighted dataset. The value in parenthesis shows the normalised Manhattan distance (M_{norm}). The closer
604 M_{norm} is to 1, the most similar to Melimoyu (highlighted in bold). The node number indicates the
605 different levels of similarity between a given cluster and the smaller cluster that contains Melimoyu
606 (Node 1). The asterisk indicates if a volcano has $\text{VEI} \geq 4$ Holocene eruptions records in the VOTW or
607 LaMEVE database.

608 *5.4 Analogue selection for Melimoyu*

609 The sensitivity analysis shows that the quality of the results, in terms of clustering performance, is very
610 similar for the three datasets, with slightly higher values of the agglomerative coefficient and Hopkins
611 statistic for the raw dataset. In the three cases, these internal validation metrics indicate inherent
612 clustering in the data and a strong clustering structure in the dendrograms. These results were obtained
613 using Ward's linkage method, which groups clusters with minimum total-within variance, known for
614 its tendency to produce compact clusters (Kaufman and Rousseeuw, 1991).

615 As a first step for selecting the analogues for Melimoyu, we analyse the dispersion in the absolute
616 probabilities estimated from each set of potential analogues (Fig. 2, 5, and 6). The dispersion in the
617 absolute probability shown in Figure 7 informs us about the difference in the eruptive behaviour
618 between the volcanoes in the three sets of potential analogues. The absolute probabilities for all the
619 potential analogues generated from the three different input datasets can be found in supplementary
620 material 5. As expected, the set of potential analogues derived from the weighted dataset, which was
621 tuned to obtain the lowest aggregate IQR, produced lower uncertainties, except for $\text{VEI} \geq 5$ eruptions. In
622 contrast, the set of analogues from the reduced dataset produced the most dispersed absolute
623 probabilities, indicating that the volcanoes proposed as analogues have notably different recurrence
624 rates per VEI class. Meanwhile, the dispersion from the analogues derived from the raw dataset is
625 between that of the other two datasets. We observe that the absolute probability decreases with the
626 eruption size, with a difference of several orders of magnitude between some volcanoes with $\text{VEI} \leq 1$
627 and $\text{VEI} \geq 5$.



628

629 **Fig. 7.** Comparison of the absolute annual probability (p_{ij}) per VEI for the three sets of potential
 630 volcanoes derived from the raw, reduced, and weighted dataset. The number in parentheses below the
 631 boxplots indicates the number of data points (i.e., the number of volcanoes with at least one eruption of
 632 a given VEI within the complete portion of the record in supplementary material 3). Note: y-axes are in
 633 different scales.

634 After analysing the dispersion in Figure 7, we apply the criteria for being an analogue of Melimoyu
 635 (Section 4.3). In addition to Melimoyu, we find that 20 out of 55 volcanoes, 8 out of 50 volcanoes, and
 636 13 out of 60 volcanoes obtained from the raw dataset, reduced dataset, and weighted dataset,
 637 respectively, meet these criteria (see supplementary material 5 for the three lists of potential analogues).

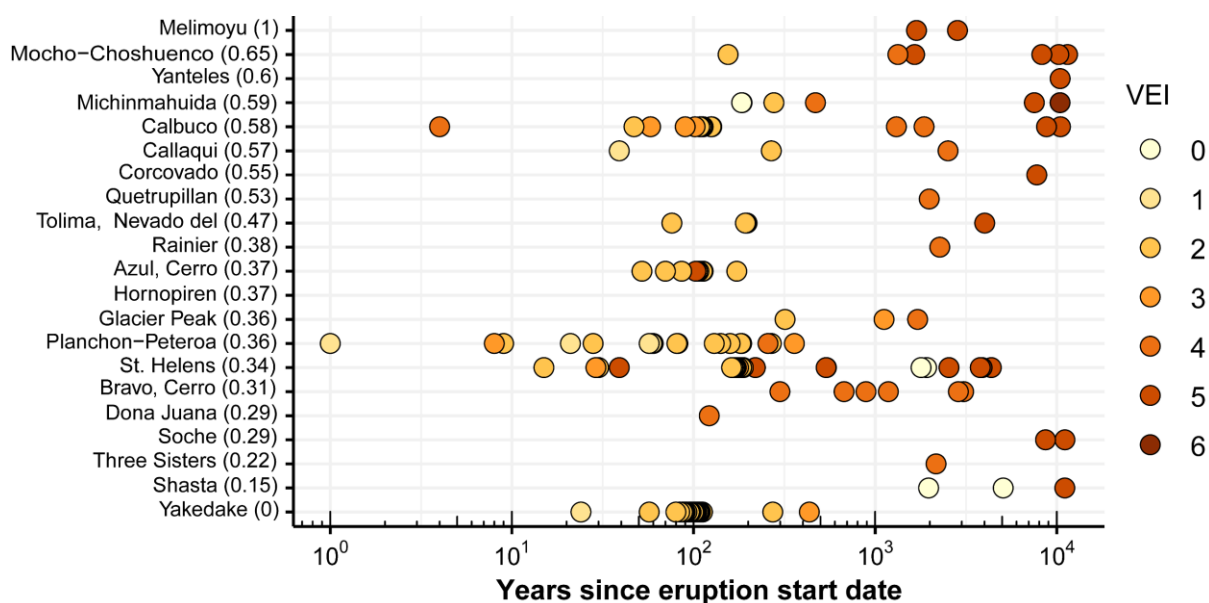
638 Due to the large dispersion in the absolute probability and the low number of volcanoes meeting the
 639 criteria, we discard the set of potential analogues derived from the reduced dataset. The other two sets
 640 of potential analogues have a similar range of absolute probabilities, although the dispersion is slightly
 641 lower for the analogues derived from the weighted dataset (Fig. 7). However, more volcanoes derived
 642 from the raw database meet the criteria for being analogues. Therefore, we retain the results from the
 643 raw dataset and conclude that it contains the best selection of analogues to calculate the empirical f - M
 644 relationship for Melimoyu.

645 The selection of 20 analogues that meet the criteria, ordered from more to less similar (i.e., highest to
 646 lowest normalised Manhattan distance in Figure 8), are Mocho-Choshuenco, Yanteles, Michinmahuida,

647 Calbuco, Callaqui, Corcovado, Quetrupillán, Nevado del Tolima, Rainier, Cerro Azul, Hornopirén,
 648 Glacier Peak, Planchón-Peteroa, St. Helens, Cerro Bravo, Doña Juana, Soche, Three Sisters, Shasta,
 649 and Yakedake. These volcanoes are located in the regions of South America (n=14), Canada and
 650 Western USA (n=5), and Honshu (n=1).

651 *5.5 Eruption probabilities for Melimoyu*

652 The eruption records from the selection of analogues derived from the raw dataset are used to calculate
 653 the empirical f - M relationship (Fig. 8). All the 20 analogues, except for Hornopirén, have at least one
 654 confirmed eruption within the complete portion of the eruption record (i.e., since the RCD in Table 2).
 655 From a total of 133 eruptions produced by all these volcanoes since the regional RCDs, nine eruptions
 656 missing in the VOTW database were added from LaMEVE, and the start date from 11 eruptions was
 657 updated with the corrected radiocarbon dates from LaMEVE. As a result of these modifications, we
 658 changed the RCD for $VEI \geq 5$ eruptions in South America, which was defined as the oldest eruption in
 659 the region (i.e., from -8460 to -9941). Therefore, the $VEI \geq 5$ absolute probabilities estimated for
 660 volcanoes in South America are slightly higher than those estimated with the updated RCD (e.g., 1.9×10^{-4}
 661 vs 1.7×10^{-4} for Michinmahuida in tabs ‘Analogues raw dataset’ and ‘Analogue selection’ in
 662 supplementary material 5).



663
 664 **Fig. 8.** Confirmed eruptions within the most complete eruption record from the analogue selection.
 665 These data were used for estimating the absolute and conditional probabilities in Figure 9. Volcanoes
 666 are listed in descending order of M_{norm} in parenthesis (i.e., more to less similar to Melimoyu). The origin
 667 of the x-axis (i.e., zero years) corresponds to 2019.

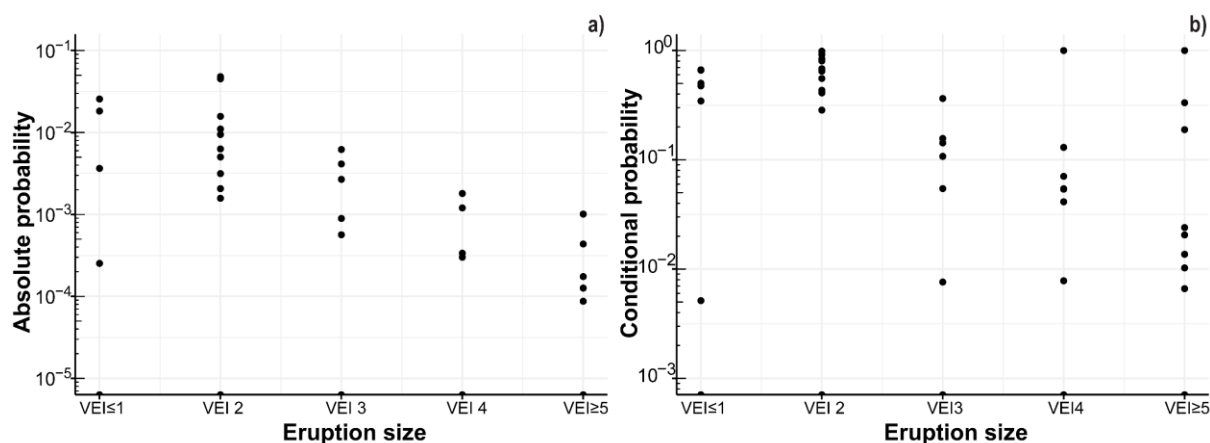
668 **Table 2.** Relative Completeness Dates (RCDs) used to calculate the probabilities in Figure 8. Dates in
 669 regular font indicate that the RCD corresponds to the most abrupt change point, dates in cursive indicate

670 that the RCD corresponds to the oldest eruption, and dates with an asterisk in cursive indicate that the
 671 RCD correspond to an alternative change point. See Burgos et al. (2022b) for method.

Region	VEI \leq 1	VEI 2	VEI 3	VEI 4	VEI \geq 5
Canada and Western USA	-5890	1820	900	-950	-5900
South America	1745*	1384	1535	-1310	-9941
Honshu	1863	1582	250	-2750	-8250

672

673 The eruption record presented in Figure 8 and the RCDs in Table 2 were used to estimate the absolute
 674 and conditional probability for each analogue (Fig. 9). We observe that, with the exception of VEI \leq 1,
 675 the absolute probability decreases as the eruption size increases (Fig. 9a). The absolute probability
 676 varies up to one order of magnitude between analogues, except for VEI \leq 1 and VEI 5 eruptions, which
 677 vary up to two orders of magnitude. Following the trend observed in Fig 9a, the overall range of
 678 conditional probabilities decreases for larger VEIs (Fig. 9b). We observe that several volcanoes, such
 679 as Corcovado, have a 100% conditional probability of VEI 4 or VEI \geq 5 eruptions because they do not
 680 have records from other eruption sizes within the complete portion of the catalogue (Fig. 8).



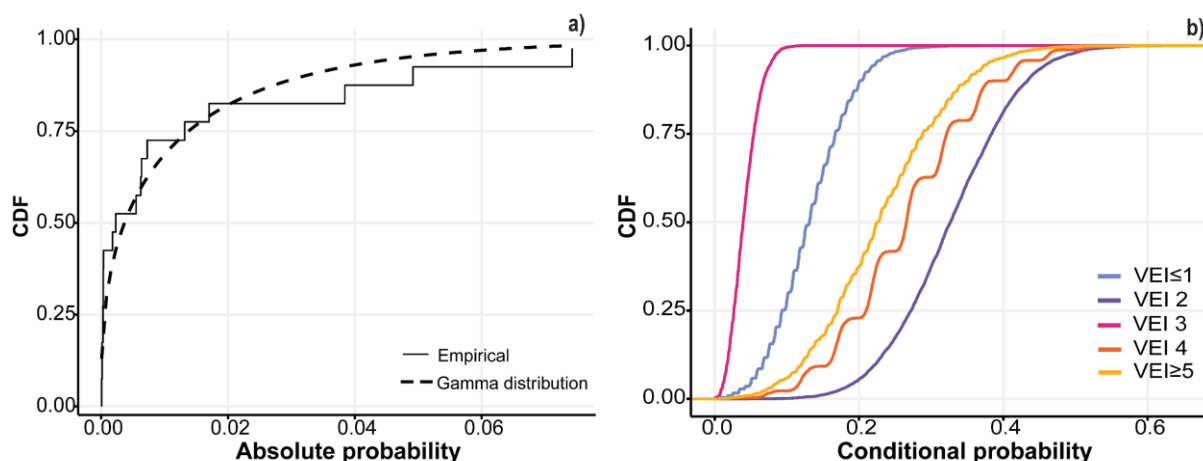
681

682 **Fig. 9.** Absolute (a) and conditional probability (b) per VEI from each volcano in the analogue selection
 683 with eruption data within the complete portion of the catalogue. The number of data points for VEI \leq 1,
 684 2, 3, 4, and \geq 5 is 6, 10, 6, 11, and 11, respectively.

685 The f - M relationship and eruption probability estimate for Melimoyu is shown in Figure 10 and Table
 686 3. The absolute probability of having an eruption of any VEI at Melimoyu can be modelled by the
 687 gamma distribution in Figure 10a with shape parameter (α) 0.369 and rate (β) 32.96. The 5th, 50th, and
 688 95th percentiles extracted from the CDF give an absolute probability of 6.55×10^{-6} , 3.68×10^{-3} , and
 689 4.78×10^{-2} , respectively. The low value of the median probability (i.e., on average, one eruption every
 690 272 years) reflects the low frequency of eruptions at Melimoyu, indicating that long periods of
 691 dormancy are common across the selection of analogues.

692 Meanwhile, the empirical CDFs in Figure 10b derived from bootstrap sampling show that the median
 693 conditional probability is the highest for VEI 2 eruptions, likely because it is the default value assigned
 694 in the VOTW database to explosive eruption without detailed descriptions (Siebert et al., 2011). The
 695 lowest conditional probabilities correspond to VEI 3 followed by $VEI \leq 1$, which might be explained by
 696 the lower number of volcanoes ($n=6$) with records from eruptions of these sizes. Assuming that an
 697 eruption occurs at Melimoyu, there is a 49% probability that the VEI is equal to or larger than four (50th
 698 percentile of the conditional probability) (Table 3). The distribution of the conditional probabilities
 699 derived from the analogue volcanoes captures the tendency to produce large explosive eruptions at
 700 Melimoyu.

701 By multiplying the absolute and conditional probability, we obtain the absolute probability of an
 702 eruption of a given VEI, which ranges from 1.45×10^{-4} for VEI 3 eruptions to 1.2×10^{-3} for VEI 2 eruptions
 703 (Table 3). The absolute probability for VEI 4 and $VEI \geq 5$ eruptions is similar, with a median average
 704 recurrence interval given by the inverse of the absolute probability of 1024 and 1204 years, respectively.



705
 706 **Fig. 10.** Cumulative Distribution Function (CDF) of the absolute probability of an eruption of any VEI
 707 (a) and empirical CDF of the conditional probability of a VEI given there is an eruption (b).

708
 709 **Table 3.** Conditional and absolute probability of having an eruption of a given VEI at Melimoyu.

	Conditional probability	Absolute probability
Eruption size	50 th percentile	50 th percentile
	[5 th ,95 th]	[5 th ,95 th]
$VEI \leq 1$	1.31×10^{-1} [5.06×10^{-2} , 2.23×10^{-1}]	4.82×10^{-4} [3.32×10^{-7} , 1.07×10^{-2}]

VEI 2	3.27×10^{-1} [1.97×10^{-1} , 4.62×10^{-1}]	1.20×10^{-3} [1.29×10^{-6} , 2.21×10^{-2}]
VEI 3	3.93×10^{-2} [1.29×10^{-2} , 7.78×10^{-2}]	1.45×10^{-4} [8.45×10^{-8} , 3.72×10^{-3}]
VEI 4	2.66×10^{-1} [1.19×10^{-1} , 4.22×10^{-1}]	9.77×10^{-4} [7.81×10^{-7} , 2.02×10^{-2}]
VEI ≥ 5	2.26×10^{-1} [8.99×10^{-2} , 3.79×10^{-1}]	8.30×10^{-4} [5.89×10^{-7} , 1.81×10^{-2}]

711 6. Discussion

712 6.1. Data availability

713 One limitation of hierarchical clustering is that it does not allow for missing values in the input data,
 714 limiting our application to complete cases (i.e., we only include volcanoes without missing data for the
 715 selected variables). Therefore, the variables and number of potential analogues used as input in the
 716 clustering are limited by the available data for each volcano. For example, when searching analogues
 717 for Melimoyu, only volcanoes in subduction zones are considered potential analogues since we include
 718 variables in the clustering that are only descriptive of this tectonic setting (e.g., the geometry of the
 719 slab). This is not considered a significant limitation in this study since the tectonic setting plays a key
 720 role in factors such as the magma budget, plumbing system configuration, and the rock composition,
 721 which partly controls the eruption style and recurrence in volcanic arcs (Acocella, 2014; Sheldrake and
 722 Caricchi, 2017; Sheldrake et al., 2020; Weber and Sheldrake, 2022). Similarly, the morphometric
 723 variables included in the global database are available only for shields, calderas, and composite
 724 volcanoes (Grosse et al., 2014; Grosse and Kervyn, 2018). Other volcano types are not included in the
 725 analysis, even though composite volcanoes, like Melimoyu, often have secondary volcanic features,
 726 such as parasitic cones and fissures. Unfortunately, these secondary features are rarely characterised
 727 and not included in global databases.

728 Not considering volcanoes in other tectonic settings or with different morphologies does not mean that
 729 they cannot be analogues of Melimoyu. These volcanoes could have been included in the clustering at
 730 the expense of excluding numerical variables that capture the variability across volcanoes within
 731 subduction zones and across composite and shield volcanoes. However, increasing the number of
 732 volcanoes included in the input data implies reducing the number of input variables since few are
 733 available across all volcanoes. For example, only the primary volcano type and tectonic setting from
 734 the VOTW database (GVP, 2013), which are categorical variables, the crustal thickness from Laske et
 735 al. (2013), and the distance to plate boundaries from Bird (2003) are available for the 1428 volcanoes
 736 listed in the global database. Even the variable rock type 1 from the VOTW database is missing for 76

737 out of 1428, meaning that rock composition would not be considered in the clustering if we included
738 all the volcanoes. A potential solution would be to identify the input dataset that maximises the number
739 of variables and volcanoes.

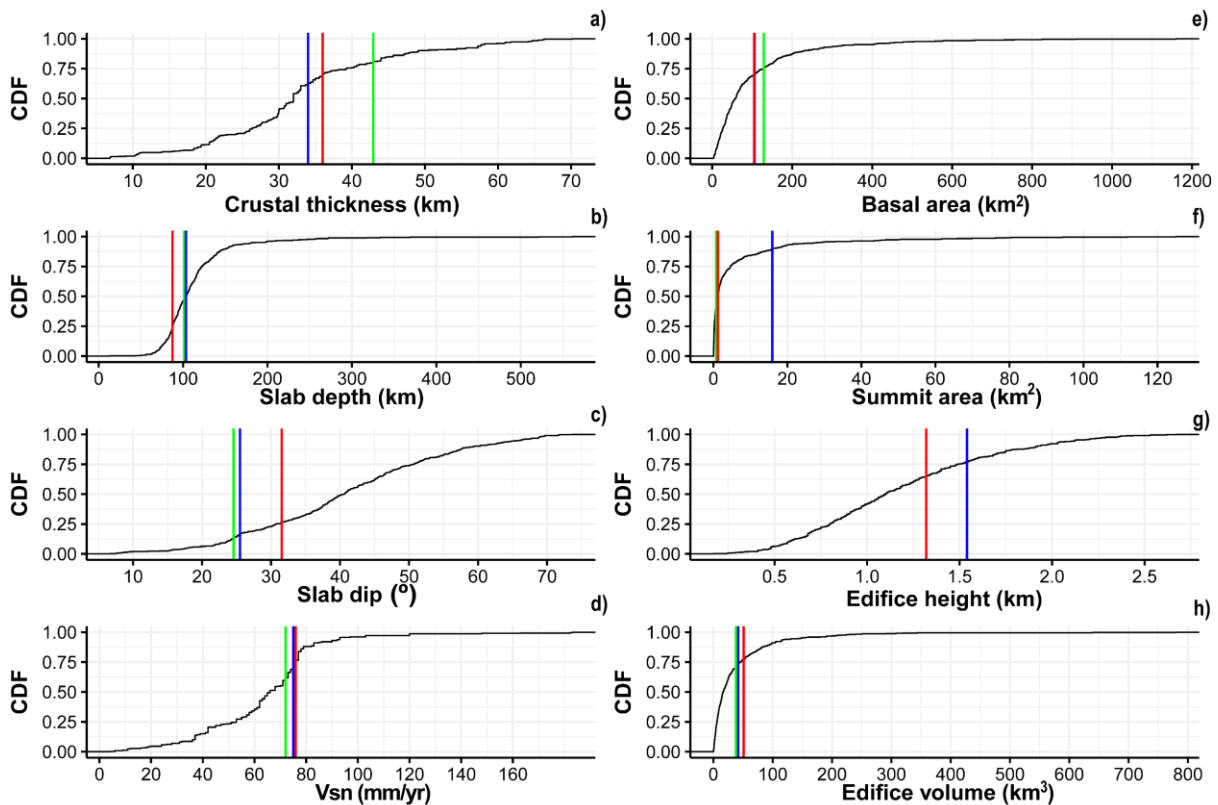
740 The flexibility of AGNES and the straightforward application allow us to adjust the variables based on
741 the available data for future applications of this approach to other target volcanoes. The number of
742 variables for target volcanoes with data mostly limited to categorical information can be increased by
743 transforming these variables into numerical variables via one-hot encoding or gathering new data (e.g.,
744 spreading rate for mid-ocean ridges or morphometric parameters for other volcano types). Alternatively,
745 other clustering algorithms that allow combining categorical and numerical variables could be tested
746 (e.g., k-prototypes), although they require pre-defining the number of clusters, adding another level of
747 iteration.

748 *6.2. Analogue suitability*

749 The dendrograms from the raw and weighted dataset (Fig. 2 and 6) indicate that the most similar
750 volcano, and, therefore, best analogue, is Mocho-Choshuenco (Chile). Mocho-Choshuenco is a
751 compound stratovolcano covered by glaciers, located 460 km from Melimoyu. The morphology of both
752 volcanoes is very similar (Fig. 11e and 11h), except for the summit area and edifice height (Fig. 11h
753 and 11g). The difference in the summit area can be explained by the fact that Grosse et al. (2013)
754 calculated the morphology of the summit of Mocho-Choshuenco including both peaks. Like Melimoyu,
755 Mocho-Choshuenco also has parasitic craters and basaltic scoria cones on the flanks, indicating
756 monogenetic volcanism (Rawson et al., 2015). Both volcanoes have similar values for multiple
757 parameters of the tectonic setting (e.g., crustal thickness, slab dip, slab depth, and normal component
758 of the velocity of the subducting plate (Fig 11a-d)). We also see a strong similarity in the rock
759 composition, with the rock types included in the GVP being identical in both volcanoes.

760 The VOTW database only reports two confirmed Holocene eruptions from Mocho-Choshuenco, the
761 most recent in 1937 of unknown eruption size. The previous eruption, reported from historical
762 observations in 1864, was classified as a VEI 2. Both eruptions were reported for Mocho stratovolcano.
763 In addition, LaMEVE reports another three Holocene eruptions dated in $1265 \text{ BP} \pm 110$, $1580 \text{ BP} \pm 115$,
764 and $8202 \text{ BP} \pm 220$, with a Magnitude of 4.6 (VEI 4), 5 (VEI 5), and 5.3 (VEI 5), respectively. Close to
765 the Holocene boundary, there are two more Plinian eruptions dated in $10189 \text{ BP} \pm 1361$ and
766 11391 ± 1002 , of Magnitude (M) 5.3 (VEI 5), and 5.7 (VEI 5), respectively. In addition to the data
767 reported in the global databases, Rawson et al. (2015) report at least 34 post-glacial explosive eruptions,
768 making Mocho-Choshuenco one of the most hazardous volcanoes from Chile in terms of the capacity
769 to produce Plinian eruptions.

770 Using the reduced dataset as input, the dendrogram (Fig. 5) shows that the most similar volcano to
 771 Melimoyu is Tolhuaca (Chile). Tolhuaca is a snow-capped stratovolcano in the vicinity of Lonquimay,
 772 also a potential analogue, 648 km from Melimoyu. We observe similar morphometric variables of
 773 Tolhuaca and Melimoyu (Fig. 11 e-h). Regarding the tectonic setting variables, both volcanoes share
 774 similar values of slab depth, slab dip, and normal component of the velocity of the subducting plate
 775 (Fig. 11b-d). The composition from the GVP indicates that Tolhuaca produces mostly Andesite/Basaltic
 776 Andesite and Basalt/Picro-Basalt, although there is evidence of Dacites (Polanco et al., 2000).
 777 According to the VOTW database, Tolhuaca has four confirmed eruptions in the Holocene, the most
 778 recent corresponding to the post-glacial (after 4000 BCE) basaltic activity (VEI 0) from the Pumehua
 779 volcanic trend located in the NW flank of Tolhuaca (Naranjo (pers, comm. 2000) in Melosh et al.
 780 (2012)). The remaining eruptions have been classified as VEI 3. There is no evidence of historical
 781 eruptions, but there is currently fumarolic activity at the summit (Polanco et al., 2000; Sanchez-Alfaro
 782 et al., 2016).



783

784 **Fig. 11.** Empirical CDF for a selection of tectonic setting parameters (a-d) and morphological
 785 parameters (e-h) from the 438 subduction zone volcanoes included in the input dataset of the clustering.
 786 The red, blue, and green lines indicate the value for Melimoyu, Mocho-Choshuenco, and Tolhuaca,
 787 respectively. Note: x-axes are in different scales.

788 The selection of the 20 analogues for Melimoyu derived from the raw dataset was made by assessing
 789 the similarity in the eruptive behaviour reflected in the dispersion of the absolute probability (Fig. 7)

790 and filtering the set of potential analogues with the set of criteria in section 4.3. The variability in the
791 results obtained from different input datasets shows the importance of combining expert knowledge
792 with quantitative and objective approaches when assessing the suitability of analogue volcanoes.

793 From the 55 potential analogues in Figure 2, 14 volcanoes were excluded because they lack confirmed
794 eruptions in the VOTW and LaMEVE database or only have eruptions without VEI, and we cannot use
795 them to estimate an f - M relationship. Therefore, 25% of the set of potential analogues are data-limited
796 volcanoes. This could be seen as a limitation in our approach since we are not excluding volcanoes with
797 scarce records from the clustering by not considering the eruptive history when defining analogues.
798 However, we think this is an advantage of our approach since it allows for finding potential analogues
799 for data-limited volcanoes and identifying where future geological studies could focus, assuming that
800 these analogues have similar eruptive behaviour, and we are missing eruptions from these data-limited
801 volcanoes. Furthermore, by not accounting for the eruptive behaviour in the input data, we can also
802 identify analogues for potentially active volcanoes. This advantage is especially important for regions
803 where eruptions from potentially active volcanoes are relatively frequent. This is the case for the
804 volcanic region of South America, where nearly 40% of all the Holocene volcanoes are potentially
805 active, and on average, a potentially active volcano has its First Recorded Eruption in the Holocene
806 (FRESH) every eight years (Burgos et al., 2022a).

807 The criteria for filtering volcanoes into the analogue selection were defined with the goal of finding
808 suitable analogues for estimating the empirical f - M relationship. This approach led to excluding Llaima
809 and Villarrica, two frequently active volcanoes with a history of large explosive eruptions ($VEI \geq 4$) in
810 the Holocene. Due to their current persistent activity and open-vent state (Ruth et al., 2016; Witter et
811 al., 2004), they cannot be considered analogues of Melimoyu in terms of eruption recurrence, especially
812 from small explosive eruptions in Villarrica (see outlier for $VEI \leq 1$ and 2 eruptions from the raw dataset
813 in Figure 7). However, the activity in Villarrica and Llaima has shifted between predominantly
814 explosive to effusive and explosive episodes over time (Lara and Clavero, 2004; Lohmar et al., 2006,
815 2005; Schindlbeck et al., 2014). These changes in eruption regimes suggest that Villarrica and Llaima
816 might be in a different life stage than Melimoyu, meaning they could be analogues over longer
817 timeframes covering regime changes with varying activity levels.

818 New methods for identifying analogues could integrate a temporal component to account for volcanic
819 system life stages and cyclical changes, moving from a static to a dynamic analogue concept. Future
820 work could explore the possibility of identifying ‘timeless’ and ‘contemporary’ analogues
821 depending on whether the variables used remain constant or change within time windows shorter
822 than the geological time scale (e.g., tectonic setting vs morphology).

823 Despite the differences in the current eruptive behaviour, the eruption history from volcanoes like
824 Villarrica and Llaima can be useful for probabilistic modelling of volcanic hazards at Melimoyu,
825 providing data that inform the range of eruption characteristics that may be expected in the future. For
826 example, eruption source parameters to model scenarios lacking in Melimoyu's records (e.g., effusive,
827 or low explosive eruptions).

828 *6.3 Importance of the tectonic setting*

829 Ten out of 20 of the analogues, including Melimoyu, are in the SVZ (Fig.1a), suggesting that the
830 characteristics of the tectonic setting strongly control the clustering. The influence that the Chile Triple
831 Junction and the LOFZ have in the nature and distribution of volcanism in the SVZ (Cembrano and
832 Lara, 2009; de Pascale et al., 2021; Gutiérrez et al., 2005; López Escobar et al., 1995; Stern et al., 2007),
833 may explain why numerous volcanoes in this area share similar characteristics with Melimoyu.

834 Similarities in the tectonic setting are also observed among the volcanic arcs where the 20 analogues
835 are located (Cascades, Northern Andes, Southern Andes, and Honshu). The range of some tectonic
836 setting variables for our analogues, such as the age of the subducting plate (from 10 to 42 Ma) or the
837 crustal thickness (from ~32 to 54 km), seems large. However, this range is relatively small compared
838 to the global values from all the volcanic arcs (~5 to 156 Ma; ~6 to 73 km). The similarity in these
839 values from analogues in distinct geographic settings shows that the clustering can identify patterns in
840 the data describing the tectonic setting while making distinctions among volcanic arcs.

841 Numerous studies have discussed the role tectonics play in the volcanism of subduction zones (e.g.,
842 Acocella (2014), Hughes and Mahood (2008, 2011), Sheldrake et al. (2020)). Heuret and Lallemand
843 (2005) and Lallemand et al. (2005) discussed the relationship between the different components of
844 subduction zones, some of which have also been found among the 438 volcanoes from our study (Fig.
845 3) (e.g., age of the subducting plate and the slab thickness). The importance of the tectonic setting in
846 the generation of different magma compositions (Hughes and Mahood, 2008, 2011; Sobradelo et al.,
847 2010; Sheldrake et al., 2020) is also reflected in the weak correlation between the crustal thickness, slab
848 dip, the normal component of the back arc strain-rate, and the presence of Basaltic and Dacitic magmas
849 (Fig. 3). The age of the subducting plate, slab and crustal thickness, subducting velocity, and
850 convergence obliquity were also highlighted by the PCA as variables contributing the most to
851 explaining the variance in PC1 (Table 1). Some of these variables also had more importance (i.e., higher
852 weights in supplementary material 4) when producing the minimum dispersion in the absolute
853 probability from the analogues derived from the weighted dataset (Fig. 7).

854 The conditions of the tectonic setting are key to developing long-lived and large plumbing systems
855 capable of generating large-magnitude explosive and caldera-forming eruptions (de Silva, 2008;
856 Hughes and Mahood, 2011, 2008b; Weber and Sheldrake, 2022). According to Sheldrake et al. (2020),

857 the crustal thickness, the age of the subducting plate, and the convergent obliquity influence the
858 production of large-magnitude eruptions ($4 \leq M \leq 7$). Their study establishes that volcanic arcs can be
859 classified into two groups with a distinct potential of having large magnitude eruptions based on the
860 parameter H (i.e., a combination of the age of the slab and movement of the subduction plate). High- H
861 regime volcanic arcs, characterised by low obliquity and moderate slab ages, are more likely to generate
862 large-magnitude eruptions. The probability of producing large-magnitude eruptions in these volcanic
863 arcs is strongly controlled by the convergent obliquity. In contrast, in low- H regime, volcanic arcs with
864 low mantle productivity and oblique convergence, the probability of generating large magnitude
865 eruptions is lower and increases with the crustal thickness. Honshu arc, where Yakedake is located, is
866 classified as High- H regime by Sheldrake et al. (2020). In contrast, the Cascades, Northern Andes, and
867 Southern Andes arcs, where 19 analogues are located, are classified by Sheldrake et al. (2020) as low-
868 H regimes and have notably similar slopes of the f - M relationship ($2.5 < \alpha < 3$ in their Figure 9d). These
869 findings further support our decision to consider these volcanoes as analogues and explain why many
870 potential analogues can produce large explosive eruptions.

871 *6.4 Uncertainty in eruption probabilities*

872 Using eruption records from multiple analogues allows for defining the uncertainty around the f - M
873 relationship estimations for Melimoyu. Relying on a small selection of analogues, as we do in this study,
874 instead of global analogues defined from broad categories, has been proven effective for reducing the
875 uncertainty in the probability estimations (Hayes et al., 2022). However, we must be cautious when
876 interpreting the range of probabilities given by the f - M relationship since, for some eruption sizes, the
877 difference between the 5th and 95th percentile can be of several orders of magnitude (Table 3). This
878 uncertainty can result from the variability in the eruption recurrence resulting from distinct eruptive
879 behaviour or different degrees of data completeness among volcanoes, which is partially accounted for
880 by using only eruption records since the RCD.

881 The discrepancies in the eruption data reported for Mocho-Choshuenco in the VOTW database, the
882 LaMEVE database, and Rawson et al. (2015) show the importance of not relying only on global
883 databases when assessing the volcanic hazard at individual volcanoes. While we used all available
884 eruption data for Melimoyu and restricted our calculation of eruption probability to only the most
885 complete portion of the VOTW database for all the analogues, we still recognise that the eruption
886 probabilities presented in this study may have been under-estimated if eruption records are missing
887 from any of the analogues. Differences among sources further support our decision to exclude the
888 eruptive history from the VOTW database in the clustering input. Under-reporting in global databases
889 can limit the ability of methods that define analogues based on eruption data from the VOTW database
890 or LaMEVE (e.g., Tierz et al. (2019) and Wang et al. (2022)) to capture all or even the most appropriate
891 analogues.

892 7. Conclusion

893 Identifying analogues for data-limited volcanoes is essential to reduce the uncertainty of volcanic
894 hazard assessments. Analogues have been typically defined using categorical information and broad
895 classes, which can lead to numerous analogues and large uncertainties in probability estimations. We
896 have combined an objective and quantitative approach to identify groups of analogues that include
897 Melimoyu, our volcano target of study, using agglomerative hierarchical clustering with an assessment
898 of suitability based on the dispersion of probability estimates and expert knowledge.

899 This algorithm was applied to 37 variables describing the tectonic setting, rock composition, and
900 morphology of 438 subduction zone volcanoes, including Melimoyu. A sensitivity analysis was
901 performed using a raw, reduced, and weighted dataset to assess how the potential analogues change
902 with the input data. We found that applying a PCA before the clustering (i.e., reduced dataset) generates
903 a group of potential analogues with highly dispersed absolute probabilities. In contrast, the dispersion
904 for the absolute probability estimated from the analogues derived from the raw and weighted dataset is
905 lower. As expected, the dispersion is the lowest for the analogues from the weighted dataset since the
906 weights were tuned to minimise the variability in the absolute probabilities across the set of analogues.

907 After applying the set of criteria deemed as important by SERNAGEOMIN and VB for estimating the
908 f - M relationship for Melimoyu (i.e., available eruption data, history of large explosive eruptions, not
909 frequently active, and a similar range of magma composition), we retain 20 analogues from the raw
910 dataset, eight from the reduced dataset, and 13 from the weighted dataset. Considering the dispersion
911 and the number of volcanoes that meet the criteria, we select the set of 20 volcanoes from the raw
912 dataset as the best analogues for Melimoyu. The clustering of these volcanoes is strongly controlled by
913 the characteristics of the tectonic setting at the volcanic arcs where they are located, which plays a key
914 role in the f - M relationships (Sheldrake et al., 2020). Furthermore, the influence of the Liquiñe-Ofqui
915 Fault Zone on the volcanism of the Southern Volcanic Zone in Chile (Cembrano and Lara, 2009; de
916 Pascale et al., 2021; Völker et al., 2011) explains why most of the analogues are from this area.

917 The f - M relationship modelled from the analogue's eruption data reflects the low frequency of eruptions
918 at Melimoyu and the history of highly explosive eruptions. For example, the probability of an eruption
919 of any VEI is 3.68×10^{-3} (50th percentile) (i.e., average recurrence interval of ~272 years), which
920 indicates long periods of recurrence between eruptions. Additionally, the conditional probability
921 distribution indicates that in the event of an eruption at Melimoyu, there is a 49% probability that it will
922 have a $VEI \geq 4$ (50th percentile), reflecting the potential for large explosive eruptions at Melimoyu.
923 Lastly, the product of the absolute and the conditional probability produces an annual probability of
924 4.8×10^{-4} , 1.2×10^{-3} , 1.5×10^{-4} , 9.8×10^{-4} , and 8.3×10^{-4} (50th percentile) for $VEI \leq 1$, 2, 3, 4, and $VEI \geq 5$
925 eruptions at Melimoyu, respectively.

926 The f -M relationship presented in this study constitutes an important step towards preparing the official
927 hazard map for Melimoyu. In addition, the probabilities and the analogues reported in this study will be
928 used by SERNAGEOMIN to establish the recurrence of different eruptive scenarios that could be
929 expected if Melimoyu reactivates. Future work will explore using the proposed analogues for Melimoyu
930 to build a probabilistic event tree and define ESP for modelling volcanic hazards.

931 This study shows that using quantitative variables when defining analogues is essential to capture the
932 diversity among volcanoes, helping to find smaller groups of volcanoes within broad categories and
933 reducing the uncertainty in the f -M relationship estimates. This approach can be combined with other
934 proposed methods and expert knowledge to fine-tune the selection of analogues. Furthermore, the
935 agglomerative hierarchical clustering can be easily applied to other volcanoes allowing the user to select
936 multiple variables from the global database made available here.

937 **8. References**

938 Abdi, H., Williams, L.J., 2010. Principal component analysis. *Wiley Interdiscip Rev Comput Stat* 2,
939 433–459. <https://doi.org/10.1002/wics.101>

940 Acocella, V., 2014. Structural control on magmatism along divergent and convergent plate
941 boundaries: Overview, model, problems. *Earth Sci Rev* 136, 226–288.
942 <https://doi.org/10.1016/j.earscirev.2014.05.006>

943 Acocella, V., di Lorenzo, R., Newhall, N., Scandone, R., 2015. An overview of recent (1988 to 2014)
944 caldera unrest: Knowledge and perspectives. *Reviews of Geophysics* 53, 896–955.
945 <https://doi.org/10.1029/88EO01108>

946 Acocella, V., Funicello, F., 2010. Kinematic setting and structural control of arc volcanism. *Earth*
947 *Planet Sci Lett* 289, 43–53. <https://doi.org/10.1016/j.epsl.2009.10.027>

948 Aggarwal, C.C., Hinneburg, A., Keim, D.A., 2001. On the Surprising Behavior of Distance Metrics
949 in High Dimensional Space, in: van den Bussche, J., Vianu, V. (Eds.), *Database Theory —*
950 *ICDT 2001*. Springer Berlin Heidelberg, Berlin, Heidelberg, pp. 420–434.
951 https://doi.org/https://doi.org/10.1007/3-540-44503-X_27

952 Assent, I., 2012. Clustering high dimensional data. *WIREs Data Mining Knowledge Discovery* 2,
953 340–350. <https://doi.org/10.1002/widm.1062>

954 Banerjee, A., Davé, R.N., 2004. Validating clusters using the Hopkins statistic, in: *IEEE International*
955 *Conference on Fuzzy Systems*. Budapest, pp. 149–153.
956 <https://doi.org/10.1109/FUZZY.2004.1375706>

- 957 Bebbington, M.S., 2014. Long-term forecasting of volcanic explosivity. *Geophys J Int* 197, 1500–
958 1515. <https://doi.org/10.1093/gji/ggu078>
- 959 Bebbington, M.S., Jenkins, S.F., 2022. Intra-Eruption Forecasting Using Analogue Volcano and
960 Eruption Sets. *J Geophys Res Solid Earth* 127. <https://doi.org/10.1029/2022JB024343>
- 961 Bird, P., 2003. An updated digital model of plate boundaries. *Geochemistry, Geophysics,*
962 *Geosystems* 4, 1027. <https://doi.org/10.1029/2001GC000252>
- 963 Boehmke, B., Greenwell, B., 2019. Hierarchical Clustering, in: *Hands-On Machine Learning with*
964 *R*. Chapman and Hall/CRC, New York. <https://doi.org/10.1201/9780367816377>
- 965 Burgos, V., Jenkins, S.F., Bebbington, M., Newhall, C., Taisne, B., 2022a. What is the probability
966 of unexpected eruptions from potentially active volcanoes or regions? *Bull Volcanol* 84, 84–
967 97. <https://doi.org/10.1007/s00445-022-01605-0>
- 968 Burgos, V., Jenkins, S.F., Bebbington, M., Newhall, C., Taisne, B., 2022b. A new perspective on
969 eruption data completeness: insights from the First Recorded EruptionS in the Holocene
970 (FRESH) database. *Journal of Volcanology and Geothermal Research* 431, 107648.
971 <https://doi.org/10.1016/j.jvolgeores.2022.107648>
- 972 Cembrano, J., Lara, L., 2009. The link between volcanism and tectonics in the southern volcanic
973 zone of the Chilean Andes: A review. *Tectonophysics* 471, 96–113.
974 <https://doi.org/10.1016/j.tecto.2009.02.038>
- 975 Chen, Peter.Y., Popovich, Paula.M., 2002. *Correlation : Parametric and Nonparametric Measures.*
976 *Sage University Papers Series on Quantitative Applications in the Social Sciences* 07–139.
- 977 Crossweller, H.S., Arora, B., Brown, S.K., Cottrell, E., Deligne, N.I., Guerrero, N.O., Hobbs, L.,
978 Kiyosugi, K., Loughlin, S.C., Lowndes, J., Nayembil, M., Siebert, L., Sparks, R.S.J.,
979 Takarada, S., Venzke, E., 2012. Global database on large magnitude explosive volcanic
980 eruptions (LaMEVE). *Journal of Applied Volcanology* 1, 1–13.
981 <https://doi.org/10.1186/2191-5040-1-4>
- 982 Daros Idalino, F., Kellem da Rosa, K., Ferrando Acuña, F., Kozhikkodan Veetil, B., Cardia Simões,
983 J., Souza, E., 2020. Recent glacier variations on Mount Melimoyu (44°50'S-72°51'W),
984 Chilean Patagonia, using Sentinel-2 data. *Geocarto Int* 35, 1199–1213.
985 <https://doi.org/10.1080/10106049.2018.1557262>
- 986 de Pascale, G.P., Froude, M., Penna, I., Hermanns, R.L., Sepúlveda, S.A., Moncada, D., Persico, M.,
987 Easton, G., Villalobos, A., Gutiérrez, F., 2021. Liqueñe-Ofqui's fast slipping intra-volcanic

- 988 arc crustal faulting above the subducted Chile Ridge. *Sci Rep* 11, 1–12.
989 <https://doi.org/10.1038/s41598-021-86413-w>
- 990 de Silva, S., 2008. Arc magmatism, calderas, and supervolcanoes. *Geology* 36, 671–672.
991 <https://doi.org/10.1130/focus082008.1>
- 992 Duque, A., González, K., Pérez, N., Benítez, D.S., 2020. Understanding the Cotopaxi Volcano
993 Activity with Clustering-Based Approaches, in: Orjuela-Cañón, A.D., Lopez, J., Arias-
994 Londoño, J.D., Figueroa-García, J.C. (Eds.), *IEEE Colombian Conference on Applications
995 in Computational Intelligence, Communications in Computer and Information Science*.
996 Springer International Publishing, Cham, pp. 3–15. [https://doi.org/10.1007/978-3-030-
997 69774-7](https://doi.org/10.1007/978-3-030-69774-7)
- 998 Geoffroy, C., 2017. Eruptive parameters and pre-eruptive processes for late Holocene activity
999 centred at Melimoyu Volcano, Southern Chile (44°05' S) (Master thesis). Universidad de
1000 Chile, Santiago de Chile.
- 1001 Geoffroy, C., Amigo, A., 2015. Avances en la Caracterización Tefrocronológica de la Actividad
1002 Explosiva Post-Glacial del Volcán Melimoyu, Chile, in: XIV Congreso Geológico Chileno.
1003 La Serena, pp. 194–197.
- 1004 Geoffroy, C.A., Alloway, B. v., Amigo, À., Parada, M.A., Gutierrez, F., Castruccio, A., Pearce,
1005 N.J.G., Morgado, E., Moreno, P.I., 2018. A widespread compositionally bimodal tephra
1006 sourced from Volcán Melimoyu (44° S, Northern Patagonian Andes): Insights into magmatic
1007 reservoir processes and opportunities for regional correlation. *Quat Sci Rev* 100, 149–151.
1008 <https://doi.org/https://doi.org/10.1016/j.quascirev.2018.09.034>
- 1009 Grosse, P., Euillades, P.A., Euillades, L.D., van Wyk de Vries, B., 2014. A global database of
1010 composite volcano morphometry. *Bull Volcanol* 76, 1–16. [https://doi.org/10.1007/s00445-
1011 013-0784-4](https://doi.org/10.1007/s00445-013-0784-4)
- 1012 Grosse, P., Kervyn, M., 2018. Morphometry of terrestrial shield volcanoes. *Geomorphology* 304, 1–
1013 14. <https://doi.org/10.1016/j.geomorph.2017.12.017>
- 1014 Gutiérrez, F., Gioncada, A., González Ferran, O., Lahsen, A., Mazzuoli, R., 2005. The Hudson
1015 Volcano and surrounding monogenetic centres (Chilean Patagonia): An example of
1016 volcanism associated with ridge-Trench collision environment. *Journal of Volcanology and
1017 Geothermal Research* 145, 207–233. <https://doi.org/10.1016/j.jvolgeores.2005.01.014>
- 1018 GVP, 2013. *Volcanoes of the World* (v. 4.8.5; 11 Feb 2020). Venzke E, editor. Smithsonian
1019 Institution. <https://doi.org/doi.org/10.5479/si.GVP.VOTW4-2013>

- 1020 GVP, 2010. Report on Melimoyu (Chile). In: Sennert, S K (ed.), Weekly Volcanic Activity Report,
1021 9 June-15 June 2010. [WWW Document]. Smithsonian Institution and US Geological
1022 Survey.
- 1023 Han, J., Kamber, M., Pei, J., 2012. Data Preprocessing, in: Jiawei Han, Micheline Kamber, J.P. (Ed.),
1024 Data Mining: Concepts and Techniques. Morgan kaufmann, pp. 83–124.
1025 <https://doi.org/https://doi.org/10.1016/B978-0-12-381479-1.00003-4>.
- 1026 Hayes, G., 2018. Slab2: A Comprehensive Subduction Zone Geometry Model [WWW Document].
1027 U.S. Geological Survey data release. URL
1028 <https://www.sciencebase.gov/catalog/item/5aa1b00ee4b0b1c392e86467> (accessed 8.11.21).
- 1029 Hayes, G.P., Moore, G.L., Portner, D.E., Hearne, M., Flamme, H., Furtney, M., Smoczyk, G.M.,
1030 2018. Slab2, a comprehensive subduction zone geometry model. *Science* (1979) 362, 58–
1031 61. [https://doi.org/DOI: 10.1126/science.aat4723](https://doi.org/DOI:10.1126/science.aat4723)
- 1032 Hayes, J.L., Jenkins, S.F., Joffrain, M., 2022. Large Uncertainties Are Pervasive in Relationships for
1033 Volcanoes in Southeast Asia. *Frontier in Earth Science* 10, 1–19.
1034 <https://doi.org/10.3389/feart.2022.895756>
- 1035 Herman, F., Brandon, M., 2015. Mid-latitude glacial erosion hotspot related to equatorial shifts in
1036 southern Westerlies. *Geology* 43, 987–990. <https://doi.org/10.1130/G37008.1>
- 1037 Heuret, A., 2006. Dynamique des zones de subduction: étude statistique globale et approche
1038 analogique. Université Montpellier II.
- 1039 Heuret, A., Lallemand, S., 2005. Plate motions, slab dynamics and back-arc deformation. *Physics of*
1040 *the Earth and Planetary Interiors* 149, 31–51. <https://doi.org/10.1016/j.pepi.2004.08.022>
- 1041 Hone, D.W.E., Mahony, S.H., Sparks, R.S.J., Martin, K.T., 2007. Cladistic analysis applied to the
1042 classification of volcanoes. *Bull Volcanol* 70, 203–220. [https://doi.org/10.1007/s00445-007-](https://doi.org/10.1007/s00445-007-0132-7)
1043 [0132-7](https://doi.org/10.1007/s00445-007-0132-7)
- 1044 Hughes, G.R., Mahood, G.A., 2011. Silicic calderas in arc settings: Characteristics, distribution, and
1045 tectonic controls. *Bulletin of the Geological Society of America* 123, 1577–1595.
1046 <https://doi.org/10.1130/B30232.1>
- 1047 Hughes, G.R., Mahood, G.A., 2008a. Tectonic controls on the nature of large silicic calderas in
1048 volcanic arcs. *Geology* 36, 627–630. <https://doi.org/10.1130/G24796A.1>
- 1049 Hughes, G.R., Mahood, G.A., 2008b. Tectonic controls on the nature of large silicic calderas in
1050 volcanic arcs. *Geology* 36, 627–630. <https://doi.org/10.1130/G24796A.1>
- 1051 Instituto Nacional de Estadísticas, 2019. Síntesis de Resultados Censo 2017, Región de Ayesén.

- 1052 Jenkins, S., Magill, C., McAneney, J., Blong, R., 2012a. Regional ash fall hazard I: A probabilistic
1053 assessment methodology. *Bull Volcanol* 74, 1699–1712. [https://doi.org/10.1007/s00445-](https://doi.org/10.1007/s00445-012-0627-8)
1054 [012-0627-8](https://doi.org/10.1007/s00445-012-0627-8)
- 1055 Jenkins, S., McAneney, J., Magill, C., Blong, R., 2012b. Regional ash fall hazard II: Asia-Pacific
1056 modelling results and implications. *Bull Volcanol* 74, 1713–1727.
1057 <https://doi.org/10.1007/s00445-012-0628-7>
- 1058 Jenkins, S.F., Biass, S., Williams, G.T., Hayes, J.L., Tennant, E., Yang, Q., Burgos, V., Meredith,
1059 E.S., Lerner, G.A., Syarifuddin, M., Verolino, A., 2022. Evaluating and ranking Southeast
1060 Asia’s exposure to explosive volcanic hazards. *Natural Hazards and Earth System Sciences*
1061 22, 1233–1265. <https://doi.org/10.5194/nhess-22-1233-2022>
- 1062 Jolliffe, I.T., Cadima, J., 2016. Principal component analysis: A review and recent developments.
1063 *Philosophical Transactions of the Royal Society A: Mathematical, Physical and Engineering*
1064 *Sciences* 374. <https://doi.org/10.1098/rsta.2015.0202>
- 1065 Kaufman, L., Rousseeuw, P.J., 1991. Chapter 5: Agglomerative Nesting (Program AGNES), in:
1066 *Finding Groups in Data: An Introduction to Cluster Analysis*. John Wiley & Sons, Inc.,
1067 Hoboken, New Jersey, pp. 199–252.
- 1068 Lallemand, S., Heuret, A., Boutelier, D., 2005. On the relationships between slab dip, back-arc stress,
1069 upper plate absolute motion, and crustal nature in subduction zones. *Geochemistry,*
1070 *Geophysics, Geosystems* 6. <https://doi.org/10.1029/2005GC000917>
- 1071 Lara, L.E., Clavero, J., 2004. Villarrica Volcano (39.5 S), Southern Andes, Chile, Jorge Clavero.
1072 *Servicio Nacional de Geología y Minería*.
- 1073 Laske, G., Masters, G., Ma, Z., Pasyanos, M., 2013. Update on CRUST1.0: A 1-degree global model
1074 of Earth’s crust, in: *EGU General Assembly 2013*. p. 2658.
- 1075 Lawson, R.G., Jurs, P.C., 1990. New index for clustering tendency and its application to chemical
1076 problems. *Journal of chemical information and computer science* 30, 36–41.
1077 <https://doi.org/https://doi.org/10.1021/ci00065a010>
- 1078 Lindsay, J.M., Robertson, R.E.A., 2018. Integrating volcanic hazard data in a systematic approach
1079 to develop volcanic hazard maps in the lesser antilles. *Front Earth Sci (Lausanne)* 6.
1080 <https://doi.org/10.3389/feart.2018.00042>
- 1081 Lohmar, S., Parada, M.Á., Robin, C., Gerbe, M.C., Deniel, C., Gourgaud, A., López-Escobar, L.,
1082 Moreno, H., Naranjo, J.A., 2006. Origin of postglacial “Mafic” ignimbrites at Llaima and

- 1083 Villarrica volcanoes (Southern Andes, Chile): Assimilation of plutonic rocks as one of the
1084 triggering factors? *Simposio Sudamericano de Geología Isotópica (SSAGI) 5*, 417–421.
- 1085 Lohmar, S., Robin, C., Parada, M.A., Gourgaud, A., Lopez-Escobar, L., Moreno, H., Naranjo, J.,
1086 2005. The two major postglacial (13-14,000 BP) pyroclastic eruptions of Llaima and
1087 Villarrica volcanoes (Southern Andes): A comparison, in: *6th International Symposium on
1088 Andean Geodynamics*. Barcelona, pp. 442–445.
- 1089 López Escobar, Á., Cembrano, J., Moreno, H., 1995. Geochemistry and tectonics of the Chilean
1090 Southern Andes basaltic Quaternary volcanism (37-46°S). *Andean Geology* 22, 219–234.
1091 <https://doi.org/10.5027/andgeoV22n2-a06>
- 1092 Loughlin, Sparks, R.S.J., Brown, S.K., Jenkins, S. F., Vye-Brown, C., 2015. Global volcanic hazards
1093 and risk, *Global Volcanic Hazards and Risk*. Cambridge University Press.
1094 <https://doi.org/10.1017/CBO9781316276273>
- 1095 Marín, A., 2014. Palena, Quitralco y Melimoyu: Intentos fallidos de colonización en el litoral de la
1096 Región de Aysén (1889-1983). *Revista Austral de Ciencias Sociales* 137–156.
1097 <https://doi.org/10.4206/rev.austral.cienc.soc.2014.n27-06>
- 1098 Marzocchi, W., Sandri, L., Gasparini, P., Newhall, C., Boschi, E., 2004. Quantifying probabilities of
1099 volcanic events: The example of volcanic hazard at Mount Vesuvius. *J Geophys Res Solid
1100 Earth* 109, 1–18. <https://doi.org/10.1029/2004JB003155>
- 1101 Mastin, L.G., Guffanti, M., Servranckx, R., Webley, P., Barsotti, S., Dean, K., Durant, A., Ewert,
1102 J.W., Neri, A., Rose, W.I., Schneider, D., Siebert, L., Stunder, B., Swanson, G., Tupper, A.,
1103 Volentik, A., Waythomas, C.F., 2009. A multidisciplinary effort to assign realistic source
1104 parameters to models of volcanic ash-cloud transport and dispersion during eruptions.
1105 *Journal of Volcanology and Geothermal Research* 186, 10–21.
1106 <https://doi.org/10.1016/j.jvolgeores.2009.01.008>
- 1107 McInnes, L., Healy, J., Melville, J., 2020. UMAP: Uniform Manifold Approximation and Projection
1108 for Dimension Reduction. *arXiv preprint arXiv:1802.03426*.
- 1109 Mead, S., Magill, C., 2014. Determining change points in data completeness for the Holocene
1110 eruption record. *Bull Volcanol* 76. <https://doi.org/10.1007/s00445-014-0874-y>
- 1111 Melnick, D., Maldonado, V., Contreras, M., 2020. Database of active and potentially-active
1112 continental faults in Chile at 1:25,000 scale. PANGAEA.

- 1113 Melosh, G., Moore, J., Stacey, R., 2012. Natural Reservoir Evolution in The Tolhuaca Geothermal
1114 Field, Southern Chile. PROCEEDINGS, Thirty-Sixth Workshop on Geothermal Reservoir
1115 Engineering.
- 1116 Mohamad, I. Bin, Usman, D., 2013. Standardization and its effects on K-means clustering algorithm.
1117 Research Journal of Applied Sciences, Engineering and Technology 6, 3299–3303.
1118 <https://doi.org/10.19026/rjaset.6.3638>
- 1119 Naranjo, J.A., Stern, C.R., 2004. Holocene tephrochronology of the southernmost part (42°30'–45°S)
1120 of the Andean Southern Volcanic Zone. Revista Geologica de Chile 31, 225–240.
1121 <https://doi.org/10.4067/S0716-02082004000200003>
- 1122 Newhall, C.G., 1982. A method for estimating intermediate and long-term risks from volcanic
1123 activity, with an example from Mount St. Helens, Washington (No. 82-396). US Geological
1124 Survey.
- 1125 Newhall, C.G., Costa, F., Ratdomopurbo, A., Venezky, D.Y., Widiwijayanti, C., Win, N.T.Z., Tan,
1126 K., Fajiculay, E., 2017. WOVOdat – An online, growing library of worldwide volcanic
1127 unrest. Journal of Volcanology and Geothermal Research 345, 184–199.
1128 <https://doi.org/10.1016/j.jvolgeores.2017.08.003>
- 1129 Newhall, C.G., Pallister, J.S., 2015. Using Multiple Data Sets to Populate Probabilistic Volcanic
1130 Event Trees, Volcanic Hazards, Risks, and Disasters. Elsevier Inc.
1131 <https://doi.org/10.1016/B978-0-12-396453-3.00008-3>
- 1132 Paguican, E.M., Grosse, P., Fabbro, G.N., Kervyn, M., 2021. Morphometric classification and spatial
1133 distribution of Philippine volcanoes. Journal of Volcanology and Geothermal Research 418,
1134 107251. <https://doi.org/10.1016/j.jvolgeores.2021.107251>
- 1135 Polanco, E., Naranjo, J., Young, S., Moreno, H., 2000. Volcanismo Explosivo Holoceno en la
1136 Cuenca del Alto Biobio, Andes del Sur (37°45'–38°30'S), in: IX Congreso Geológico
1137 Chileno: Puerto Varas, 31 de Julio al 4 de Agosto, 2000.
- 1138 Rawson, H., Naranjo, J.A., Smith, V.C., Fontijn, K., Pyle, D.M., Mather, T.A., Moreno, H., 2015.
1139 The frequency and magnitude of post-glacial explosive eruptions at Volcán Mocho-
1140 Choshuenco, southern Chile. Journal of Volcanology and Geothermal Research 299, 103–
1141 129. <https://doi.org/10.1016/j.jvolgeores.2015.04.003>
- 1142 Rodado, A., Bebbington, M., Noble, A., Cronin, S., Jolly, G., 2011. On Selection of Analog
1143 Volcanoes. Math Geosci 43, 505–519. <https://doi.org/10.1007/s11004-011-9345-6>

- 1144 Rojas Hoppe, C., Subiabre, A., 1998. La Carretera Austral Entre Puerto Montt y La Junta (Región
1145 Sur de Chile) y Sus Amenazas Naturales. Cuadernos de Geografía: Revista Colombiana de
1146 Geografía 7, 50–69.
- 1147 Runge, M.G., Bebbington, M.S., Cronin, S.J., Lindsay, J.M., Kenedi, C.L., Moufti, M.R.H., 2014.
1148 Vents to events: Determining an eruption event record from volcanic vent structures for the
1149 Harrat Rahat, Saudi Arabia. *Bull Volcanol* 76, 1–16. [https://doi.org/10.1007/s00445-014-](https://doi.org/10.1007/s00445-014-0804-z)
1150 [0804-z](https://doi.org/10.1007/s00445-014-0804-z)
- 1151 Sanchez-Alfaro, P., Reich, M., Arancibia, G., Pérez-Flores, P., Cembrano, J., Driesner, T., Lizama,
1152 M., Rowland, J., Morata, D., Heinrich, C.A., Tardani, D., Campos, E., 2016. Physical,
1153 chemical and mineralogical evolution of the Tolhuaca geothermal system, southern Andes,
1154 Chile: Insights into the interplay between hydrothermal alteration and brittle deformation.
1155 *Journal of Volcanology and Geothermal Research* 324, 88–104.
1156 <https://doi.org/10.1016/j.jvolgeores.2016.05.009>
- 1157 Sandri, L., Jolly, G., Lindsay, J., Howe, T., Marzocchi, W., 2012. Combining long- and short-term
1158 probabilistic volcanic hazard assessment with cost-benefit analysis to support decision
1159 making in a volcanic crisis from the Auckland Volcanic Field, New Zealand. *Bull Volcanol*
1160 74, 705–723. <https://doi.org/10.1007/s00445-011-0556-y>
- 1161 Sandri, L., Thouret, J.C., Constantinescu, R., Biass, S., Tonini, R., 2014. Long-term multi-hazard
1162 assessment for El Misti volcano (Peru). *Bull Volcanol* 76, 1–26.
1163 <https://doi.org/10.1007/s00445-013-0771-9>
- 1164 Schindlbeck, J.C., Freundt, A., Kutterolf, S., 2014. Major changes in the post-glacial evolution of
1165 magmatic compositions and pre-eruptive conditions of Llaima Volcano, Andean Southern
1166 Volcanic Zone, Chile. *Bull Volcanol* 76, 1–22. <https://doi.org/10.1007/s00445-014-0830-x>
- 1167 SERNAGEOMIN, 2019. Ranking de Riesgo Específico de Volcanes Activos de Chile 2019.
- 1168 Sheldrake, T., 2014. Long-term forecasting of eruption hazards: A hierarchical approach to merge
1169 analogous eruptive histories. *Journal of Volcanology and Geothermal Research* 286, 15–23.
1170 <https://doi.org/10.1016/j.jvolgeores.2014.08.021>
- 1171 Sheldrake, T., Caricchi, L., 2017. Regional variability in the frequency and magnitude of large
1172 explosive volcanic eruptions. *Geology* 45, 111–114. <https://doi.org/10.1130/G38372.1>
- 1173 Sheldrake, T.E., Scutari, M., Caricchi, L., 2020. Tectonic controls on global variations in the record
1174 of large-magnitude explosive eruptions in volcanic arcs. *Front Earth Sci (Lausanne)* 8, 1–14.
1175 <https://doi.org/10.3389/feart.2020.00127>

- 1176 Siebert, L., Cottrell, E., Venzke, E., Edwards, B., 2015. Catalog of Earth's Documented Holocene
1177 Eruptions, Second Edi. ed, The Encyclopedia of Volcanoes. Elsevier Inc.
1178 <https://doi.org/10.1016/b978-0-12-385938-9.15002-3>
- 1179 Siebert, L., Simkin, T., Kimberly, P., 2011. Volcanoes of the World. Univ of California Press.
- 1180 Sobradelo, R., Geyer, A., Martí, J., 2010. Statistical data analysis of the CCDB (Collapse Caldera
1181 Database): Insights on the formation of caldera systems. Journal of Volcanology and
1182 Geothermal Research 198, 241–252. <https://doi.org/10.1016/j.jvolgeores.2010.09.003>
- 1183 Solow, A.R., 2001. An Empirical Bayes Analysis of Volcanic Eruptions. Math Geol 33, 95–102.
1184 <https://doi.org/10.1023/A:1007514410745>
- 1185 Stern, C.R., De Porras, M.E., Maldonado, A., 2015. Tefrocronología en curso superior del valle del
1186 río Cisne (44°S), Chile Austral. Andean Geology 42, 173–189.
1187 <https://doi.org/10.5027/andgeoV42n2-a02>
- 1188 Stern, C.R., Moreno, H., López-Escobar, L., Clavero, J.E., Lara, L.E., Naranjo, J.A., Parada, M.A.,
1189 Skewes, M.A., 2007. Chilean volcanoes, in: Moreno, T., Gibbons, W. (Eds.), The Geology
1190 of Chile. Geological Society of London. <https://doi.org/https://doi.org/10.1144/GOCH.5>
- 1191 Strauss, T., Von Maltitz, M.J., 2017. Generalising ward's method for use with manhattan distances.
1192 PLoS One 12, 1–21. <https://doi.org/10.1371/journal.pone.0168288>
- 1193 Szakács, A., 1994. Redefining active volcanoes: a discussion. Bull Volcanol 56, 321–325.
1194 <https://doi.org/10.1007/BF00326458>
- 1195 Tennant, E., Jenkins, S.F., Winson, A., Widiwijayanti, C., Gunawan, H., Haerani, N., Kartadinata,
1196 N., Banggur, W., Triastuti, H., 2021. Reconstructing eruptions at a data limited volcano: A
1197 case study at Gede (West Java). Journal of Volcanology and Geothermal Research 418.
1198 <https://doi.org/10.1016/j.jvolgeores.2021.107325>
- 1199 Tierz, P., Clarke, B., Calder, E.S., Dessalegn, F., Lewi, E., Yirgu, G., Fontijn, K., Crummy, J.M.,
1200 Bekele, Y., Loughlin, S.C., 2020. Event Trees and Epistemic Uncertainty in Long-Term
1201 Volcanic Hazard Assessment of Rift Volcanoes: The Example of Aluto (Central Ethiopia).
1202 Geochemistry, Geophysics, Geosystems 21. <https://doi.org/10.1029/2020GC009219>
- 1203 Tierz, P., Loughlin, S.C., Calder, E.S., 2019. VOLCANS: an objective, structured and reproducible
1204 method for identifying sets of analogue volcanoes. Bull Volcanol 81.
1205 <https://doi.org/10.1007/s00445-019-1336-3>
- 1206 Unglert, K., Radić, V., Jellinek, A.M., 2016. Principal component analysis vs. self-organizing maps
1207 combined with hierarchical clustering for pattern recognition in volcano seismic spectra.

- 1208 Journal of Volcanology and Geothermal Research 320, 58–74.
1209 <https://doi.org/10.1016/j.jvolgeores.2016.04.014>
- 1210 Völker, D., Kutterolf, S., Wehrmann, H., 2011. Comparative mass balance of volcanic edifices at the
1211 southern volcanic zone of the Andes between 33°S and 46°S. Journal of Volcanology and
1212 Geothermal Research 205, 114–129. <https://doi.org/10.1016/j.jvolgeores.2011.03.011>
- 1213 Wang, T., Bebbington, M., Cronin, S., Carman, J., 2022. Forecasting Eruptions at Poorly Known
1214 Volcanoes Using Analogs and Multivariate Renewal Processes. Geophys Res Lett 49, 1–14.
1215 <https://doi.org/10.1029/2021gl096715>
- 1216 Watt, S.F.L., Pyle, D.M., Mather, T.A., 2009. The influence of great earthquakes on volcanic
1217 eruption rate along the Chilean subduction zone. Earth Planet Sci Lett 277, 399–407.
1218 <https://doi.org/10.1016/j.epsl.2008.11.005>
- 1219 Weber, G., Sheldrake, T.E., 2022. Geochemical variability as an indicator for large magnitude
1220 eruptions in volcanic arcs. Sci Rep 12, 15854. <https://doi.org/10.1038/s41598-022-19902-1>
- 1221 Weller, D.J., de Porras, M.E., Maldonado, A., Méndez, C., Stern, C.R., 2017. Tefrocronología
1222 holocena del curso inferior del valle de río Cisnes, Chile austral. Andean Geology 44, 229–
1223 248. <https://doi.org/10.5027/andgeov44n3-a01>
- 1224 Whelley, P.L., Newhall, C.G., Bradley, K.E., 2015. The frequency of explosive volcanic eruptions
1225 in Southeast Asia. Bull Volcanol 77. <https://doi.org/10.1007/s00445-014-0893-8>
- 1226 Wils, K., van Daele, M., Lastras, G., Kissel, C., Lamy, F., Siani, G., 2018. Holocene Event Record
1227 of Aysén Fjord (Chilean Patagonia): An Interplay of Volcanic Eruptions and Crustal and
1228 Megathrust Earthquakes. J Geophys Res Solid Earth 123, 324–343.
1229 <https://doi.org/10.1002/2017JB014573>
- 1230 Xu, D., Tian, Y., 2015. A Comprehensive Survey of Clustering Algorithms. Annals of Data Science
1231 2, 165–193. <https://doi.org/10.1007/s40745-015-0040-1>

1232

1233 9. Data Availability

1234 The Supplementary Materials are deposited in the NTU open access research data repository DR-NTU
1235 (Data).

1236 Supplementary material 1: <https://doi.org/10.21979/N9/9DL728>

1237 Supplementary material 2: <https://doi.org/10.21979/N9/73C0II>

1238 Supplementary material 3: <https://doi.org/10.21979/N9/CLOY0S>

1239 Supplementary material 4: <https://doi.org/10.21979/N9/ZPAN0X>

1240 Supplementary material 5: <https://doi.org/10.21979/N9/KNMKAJ>

1241 **10. Author contributions**

1242 VB, SJ, LBT, CPM, MB, CN, AA, and BT contributed to the project idea, goals, and objectives.

1243 VB developed the methodology with input from SJ, LBT, CPM, MB, JPA, and BT. VB

1244 processed the data, analysed the results, prepared the figures, and wrote the manuscript. All

1245 authors read, reviewed, and approved the final version of the manuscript.

1246 **11. Acknowledgements**

1247 We would like to thank Pablo Tierz, Tom Sheldrake, Elly Tennant, and Christina Widiwijayanti for the

1248 fruitful discussions about volcanic analogues. We are also grateful to Constanza Jorquera Flores for the

1249 numerous meetings about Melimoyu.

1250 **12. Funding**

1251 This research was supported by the Earth Observatory of Singapore via its funding from the National

1252 Research Foundation Singapore and the Singapore Ministry of Education under the Research Centres

1253 of Excellence initiative. This work comprises EOS contribution number 504. MB was supported by the

1254 Resilience to Nature's Challenges Volcano program, New Zealand (contract number GNS-RNC047).

1255